SENSITIVITIES OF SIMULATED FIRE-INDUCED FLOWS TO FIRE SHAPE AND BACKGROUND WIND PROFILE USING A CLOUD-RESOLVING MODEL

By

Marshall S. Stageberg

A THESIS

Submitted to
Michigan State University
in partial fulfillment of the requirements
for the degree of

Geography – Master of Science

2018

ABSTRACT

SENSITIVITIES OF SIMULATED FIRE-INDUCED FLOWS TO FIRE SHAPE AND BACKGROUND WIND PROFILE USING A CLOUD-RESOLVING MODEL

By

Marshall S. Stageberg

Wildland fire behavior can be very difficult to predict because of inherent non-linearities and multi-scale processes associated with fire-atmosphere interactions. Circulations and complex flows in the vicinity of a fire are driven by heat release from the fire. Since extreme conditions in the fire environment make collecting meteorological observations difficult, we employ a high-resolution numerical model to simulate the atmospheric responses to a fire. Specifically, we have chosen Cloud Model 1 (CM1) because it is designed to simulate high resolution, cloud scale processes that are comparable in scale to fire-induced flows. A surface sensible heat flux is added to CM1 to simulate the effect of a fire and the resultant fire-induced circulations and complex flows are examined. Using CM1 allows us to produce simulations with fine spatial and temporal resolution with a detailed representation of the evolution of the fire-atmosphere system.

For the purpose of this study, we perform a series of simulations to examine the sensitivity of fire-induced flows to the shape of the simulated fire and to background wind profile. We show how fire shape and the background wind profile affect the intensity and extent of fire-induced perturbations to the lower atmosphere. The results from these numerical simulations, when combined with field observations, help improve our understanding of fire-atmosphere interactions. The results from this study can potentially help fire managers with decision-making when fighting wildland fires.

This thesis is dedicated to all of my family, friends, collaborators, and mentors who have given their unconditional and continued support throughout the entire process.

Thank you

ACKNOWLEDGMENTS

I cannot thank enough my co-advisors of Dr. Joseph J. Charney, Dr. Shiyuan Zhong, and Dr. Alan F. Srock for their encouragement to pursue a graduate degree and for all of their help and support during my graduate studies. They not only provided amazing technical guidance to help me develop professional skills, but also great personal advice to make me a better person. I also would like to thank Dr. Lifeng Luo for serving on my committee and for his patience and advice to help me finish my degree. I would like to thank all of the friends I've made at Michigan State University who have given great advice that has helped me succeed.

I would like to acknowledge all of the financial support that has made this project possible, including salary provided by the Forest Service Northern Research Station and the 2017 M. Sc. Scholarship provided by the International Association of Wildland Fire. The computations would not have been possible without the resources that were made available, including the Blue Waters sustained-petascale computing project supported by the National Science Foundation (awards OCI-0725070 and ACI-1238993) and the state of Illinois, the Extreme Science and Engineering Discovery Environment (XSEDE) supported by National Science Foundation grant number ACI-1548562, and the High Performance Computer Centers at the Forest Service Northern Research Station and the Michigan State University.

Finally, I would like to thank all of my family especially my mother and father. Although my father passed away in 2014, he has been with me every step of the journey. I would also like to give a huge thank you to my ultimate supporter, my best friend, my girlfriend, Andrea Starr. Without her constant support and push I would not be where I am today. Thank you.

TABLE OF CONTENTS

LIST OF TABLES...vi

LIST OF FIGURES...vii

KEY TO ABBREVIATIONS...xii

CHAPTER I – INTRODUCTION...1

CHAPTER II - LITERATURE REVIEW...4
2.1 Theoretical and Observational Studies...4
2.1.1 Background Wind...4
2.1.2 Fire Shape...6
2.2 Numerical Studies...7
2.2.1 Past Numerical Modeling Studies...7
2.2.2 Current Numerical Modeling Study...11

CHAPTER III - SENSITIVITIES OF SIMULATED FIRE-INDUCED FLOWS TO FIRE SHAPE AND BACKGROUND WIND PROFILE USING A CLOUD-RESOLVING MODEL...13
3.1 Introduction...13
3.2 Methods...13
3.2.1 Model Setup 13
3.2.2 Model Simulations 14
3.3 Results...18
3.3.1 Vertical Cross Sections...18
3.3.2 Time Series...23
3.3.3 Surface Analysis...24
3.3.4 Vertical Vorticity...28

CHAPTER IV - DISCUSSION AND CONCLUSION...33

APPENDIX...36

BIBLIOGRAPHY...58

LIST OF TABLES

Table 1. All of the simulations analyzed are shown with their respective name and background characteristics....................17

LIST OF FIGURES

Figure 1. Three fire shapes (shape A, shape B, and shape C) and their location within the model domain. The locations where a sensible heat flux of 25 kW m^{-2} is applied are shaded in red......15

Figure 2. Three background wind profile that are used in the simulations: no background wind (black), 5 m s^{-1} max wind (blue), 10 m s^{-1} max wind (red)...16

Figure 3. Vertical cross section of u-wind 1700 s into the simulations. u-wind velocities are shaded. Positive values indicate a wind direction to the right, negative values indicate a wind direction to the left...20

Figure 4. Cross section of vertical velocity 1700 s into the simulations. Vertical velocities are shaded. Positive values indicate an upward wind, negative values indicate a downward wind...22

Figure 5. Time series of the maximum plume height for all of the simulations...........................23

Figure 6. Horizontal cross section of the perturbation of u-winds at the surface 1700 s into the simulations. The perturbation of u-winds at the surface are shaded. Positive values indicate a wind direction to the right, negative values indicate a wind direction to the left.........................25

Figure 7. Horizontal cross section of divergence at the surface 1700 s into all of the simulations. Divergence is shaded by positive values, convergence is shaded by negative values..................27

Figure 8. Timeseries of domain wide vertical vorticity distributions. The vertical vorticity values greater/less than +/- 0.25 s^{-1} are analyzed in the distribution. The min/max (dark blue), 95th percentile (shaded teal), 25th percentile (black), and mean (shaded purple).................................29

Figure 9. Horizontal cross section of vertical vorticity at the surface 1700 s into all of the simulations. Positive values of vertical vorticity indicate cyclonic rotation, and negative values of vertical vorticity indicate anticyclonic rotation...32

Figure A1. Horizontal cross section of the perturbation of u-winds at the surface 600 s into the simulations. The perturbation of u-winds at the surface are shaded. Positive values indicate a wind direction to the right, negative values indicate a wind direction to the left.........................37

Figure A2. Horizontal cross section of the perturbation of u-winds at the surface 1200 s into the simulations. The perturbation of u-winds at the surface are shaded. Positive values indicate a wind direction to the right, negative values indicate a wind direction to the left.........................38

Figure A3. Horizontal cross section of divergence at the surface 600 s into the simulations. Divergence is shaded by positive values, convergence is shaded by negative values..................39

Figure A4. Horizontal cross section of divergence at the surface 1200 s into the simulations. Divergence is shaded by positive values, convergence is shaded by negative values..................40

Figure A5. Horizontal cross section of vertical vorticity at the surface 600 s into the simulations. Positive values of vertical vorticity indicate cyclonic rotation, and negative values of vertical vorticity indicate anticyclonic rotation...41

Figure A6. Horizontal cross section of vertical vorticity at the surface 1200 s into the simulations. Positive values of vertical vorticity indicate cyclonic rotation, and negative values of vertical vorticity indicate anticyclonic rotation...42

Figure A7. Vertical cross section through the middle of the domain. The y component of vorticity for the 0ShapeA simulation is shaded. Positive values of y-vorticity indicate cyclonic rotation about the y-axis, and negative values of y-vorticity indicate anticyclonic rotation about the y-axis...43

Figure A8. Vertical cross section through the middle of the domain. The x component of vorticity for the 0ShapeA simulation is shaded Positive values of x-vorticity indicate cyclonic rotation about the x-axis, and negative values of x-vorticity indicate anticyclonic rotation about the x-axis...43

Figure A9. Horizontal cross section of the v-winds at the surface 600, 1200, 1700 s respectively into the 0ShapeA simulation. The v-winds at the surface are shaded. Positive values indicate a wind direction from the bottom to the top of the image, negative values indicate a wind direction from the top to the bottom of the image. Convergence of the winds inside the fire arc is associated with the same location of the vertical vorticity minimum/maximum features............44

Figure A10. Vertical cross section of y-vorticity at x = 285 (150 m upwind of the front of the fire). The y component of vorticity for the 5ShapeA simulation is shaded such that positive values of y-vorticity indicate cyclonic rotation about the y-axis, and negative values of y-vorticity indicate anticyclonic rotation about the y-axis...44

Figure A11. Vertical cross section of x-vorticity through the center of the domain. The x component of vorticity for the 5ShapeA simulation is shaded such that positive values of x-vorticity indicate cyclonic rotation about the x-axis, and negative values of x-vorticity indicate anticyclonic rotation about the x-axis...45

Figure A12. Horizontal cross section of the v-winds at the surface 600, 1200, 1700 s respectively into the 5ShapeA simulation. The v-winds at the surface are shaded. Positive values indicate a wind direction from the bottom to the top of the image, negative values indicate a wind direction from the top to the bottom of the image. Convergence of the winds inside the fire arc is associated with the same location of the vertical vorticity minimum/maximum features............45

Figure A13. Vertical cross section of y-vorticity at x = 285 (150 m upwind of the front of the fire). The y component of vorticity for the 10ShapeA simulation is shaded such that positive values of y-vorticity indicate cyclonic rotation about the y-axis, and negative values of y-vorticity indicate anticyclonic rotation about the y-axis...46

Figure A14. Vertical cross section of x-vorticity through the center of the domain. The x component of vorticity for the 10ShapeA simulation is shaded such that positive values of x-vorticity indicate cyclonic rotation about the x-axis, and negative values of x-vorticity indicate anticyclonic rotation about the x-axis...46

Figure A15. Horizontal cross section of the v-winds at the surface 600, 1200, 1700 s respectively into the 10ShapA simulation. The v-winds at the surface are shaded. Positive values indicate a wind direction from the bottom to the top of the image, negative values indicate a wind direction from the top to the bottom of the image. Convergence of the winds outside the fire arc is associated with the same location of the vertical vorticity minimum/maximum features............47

Figure A16. Vertical cross section of y-vorticity at x = 285 (150 m upwind of the front of the fire). The y component of vorticity for the 0ShapeB simulation is shaded such that positive values of y-vorticity indicate cyclonic rotation about the y-axis, and negative values of y-vorticity indicate anticyclonic rotation about the y-axis..47

Figure A17. Vertical cross section of x-vorticity through the center of the domain. The x component of vorticity for the 0ShapeB simulation is shaded such that positive values of x-vorticity indicate cyclonic rotation about the x-axis, and negative values of x-vorticity indicate anticyclonic rotation about the x-axis..48

Figure A18. Horizontal cross section of the v-winds at the surface 600, 1200, 1700 s respectively into the 0ShapeB simulation. The v-winds at the surface are shaded. Positive values indicate a wind direction from the bottom to the top of the image, negative values indicate a wind direction from the top to the bottom of the image. Convergence of the winds inside the fire arc is associated with the same location of the vertical vorticity minimum/maximum features............48

Figure A19. Vertical cross section of y-vorticity at x = 285 (150 m upwind of the front of the fire). The y component of vorticity for the 5ShapeB simulation is shaded such that positive values of y-vorticity indicate cyclonic rotation about the y-axis, and negative values of y-vorticity indicate anticyclonic rotation about the y-axis..49

Figure A20. Vertical cross section of x-vorticity through the center of the domain. The x component of vorticity for the 5ShapeB simulation is shaded such that positive values of x-vorticity indicate cyclonic rotation about the x-axis, and negative values of x-vorticity indicate anticyclonic rotation about the x-axis..49

Figure A21. Horizontal cross section of the v-winds at the surface 600, 1200, 1700 s respectively into the 5ShapeB simulation. The v-winds at the surface are shaded. Positive values indicate a wind direction from the bottom to the top of the image, negative values indicate a wind direction from the top to the bottom of the image. Convergence of the winds inside the fire arc is associated with the same location of the vertical vorticity minimum/maximum features...50

Figure A22. Vertical cross section of y-vorticity at x = 285 (150 m upwind of the front of the fire). The y component of vorticity for the 10ShapeB simulation is shaded such that positive values of y-vorticity indicate cyclonic rotation about the y-axis, and negative values of y-vorticity indicate anticyclonic rotation about the y-axis..50

Figure A23. Vertical cross section of x-vorticity through the center of the domain. The x component of vorticity for the 10ShapeB simulation is shaded such that positive values of x-vorticity indicate cyclonic rotation about the x-axis, and negative values of x-vorticity indicate anticyclonic rotation about the x-axis..51

Figure A24. Horizontal cross section of the v-winds at the surface 600, 1200, 1700 s respectively into the 10ShapeB simulation. The v-winds at the surface are shaded. Positive values indicate a wind direction from the bottom to the top of the image, negative values indicate a wind direction from the top to the bottom of the image. Convergence of the winds outside the fire arc is associated with the same location of the vertical vorticity minimum/maximum features...51

Figure A25. Vertical cross section of x-vorticity through the center of the domain. The x component of vorticity for the 0ShapeC simulation is shaded such that positive values of x-vorticity indicate cyclonic rotation about the x-axis, and negative values of x-vorticity indicate anticyclonic rotation about the x-axis..52

Figure A26. Vertical cross section of y-vorticity at x = 285 (150 m upwind of the front of the fire). The y component of vorticity for the 0ShapeC simulation is shaded such that positive values of y-vorticity indicate cyclonic rotation about the y-axis, and negative values of y-vorticity indicate anticyclonic rotation about the y-axis...52

Figure A27. Horizontal cross section of the v-winds at the surface 600, 1200, 1700 s respectively into the 0ShapeC simulation. The v-winds at the surface are shaded. Positive values indicate a wind direction from the bottom to the top of the image, negative values indicate a wind direction from the top to the bottom of the image. Convergence of the winds inside the fire arc is associated with the same location of the vertical vorticity minimum/maximum features...53

Figure A28. Vertical cross section of y-vorticity at x = 285 (150 m upwind of the front of the fire). The y component of vorticity for the 5ShapeC simulation is shaded such that positive values of y-vorticity indicate cyclonic rotation about the y-axis, and negative values of y-vorticity indicate anticyclonic rotation about the y-axis...53

Figure A29. Vertical cross section of x-vorticity through the center of the domain. The x component of vorticity for the 5ShapeC simulation is shaded such that positive values of x-vorticity indicate cyclonic rotation about the x-axis, and negative values of x-vorticity indicate anticyclonic rotation about the x-axis..54

Figure A30. Horizontal cross section of the v-winds at the surface 600, 1200, 1700 s respectively into the 5ShapeC simulation. The v-winds at the surface are shaded. Positive values indicate a wind direction from the bottom to the top of the image, negative values indicate a wind direction from the top to the bottom of the image. Convergence of the winds inside the fire arc is associated with the same location of the vertical vorticity minimum/maximum features.............54

Figure A31. Vertical cross section of y-vorticity at x = 285 (150 m upwind of the front of the fire). The y component of vorticity for the 10ShapeC simulation is shaded such that positive values of y-vorticity indicate cyclonic rotation about the y-axis, and negative values of y-vorticity indicate anticyclonic rotation about the y-axis..55

Figure A32. Vertical cross section of x-vorticity through the center of the domain. The x component of vorticity for the 10ShapeC simulation is shaded such that positive values of x-vorticity indicate cyclonic rotation about the x-axis, and negative values of x-vorticity indicate anticyclonic rotation about the x-axis..55

Figure A33. Horizontal cross section of the v-winds at the surface 600, 1200, 1700 s respectively into the 10ShapeC simulation. The v-winds at the surface are shaded. Positive values indicate a wind direction from the bottom to the top of the image, negative values indicate a wind direction from the top to the bottom of the image. Convergence of the winds outside the fire arc is associated with the same location of the vertical vorticity minimum/maximum features. Linear bands of convergence form throughout the simulation that are associated with the linear bands of convergence seen in the u-wind...56

Figure A34. Upwind view of a three-dimensional volume render of vertical vorticity at 600, 1200, 1700 s into the 10ShapeC simulations. The surface is shaded by the perturbations from background u-wind and the volume is shaded by values of vertical vorticity. Positive values of vertical vorticity indicate cyclonic rotation, and negative values of vertical vorticity indicate anticyclonic rotation...57

Figure A35. Oblique view of a three-dimensional volume render of vertical vorticity at 600, 1200, 1700 s into the 10ShapeC simulations. The surface is shaded by the perturbations from background u-wind and the volume is shaded by values of vertical vorticity. Positive values of vertical vorticity indicate cyclonic rotation, and negative values of vertical vorticity indicate anticyclonic rotation...57

KEY TO ABBREVIATIONS

AGL – above ground level

ARPS – Advanced Regional Prediction System

CM1 – Cloud Model 1

FDS – Fire Dynamics Simulator

ft – feet

hPa – hectopascal(s)

kW m^{-2} – kilowatts per meter squared

LES – large-eddy simulation

m – meter(s)

m s^{-1} – meters per second

s – second(s)

UU-LES – University of Utah large-eddy simulation

WFDS – WUI Fire Dynamics Simulator

WRF – Weather Research and Forecasting

WUI – Wildland urban interface

CHAPTER I – INTRODUCTION

Wildland fires impact atmospheric circulations when heat and moisture released by combustion induces an atmospheric response. The response has the potential to interact with the fire over a range of spatial and temporal scales. When investigating the atmospheric response to a wildland fire, the circulations can be difficult to study due to non-linearities and multi-scale processes associated with combustion. Combustion is a molecular process in which heat and moisture are released on scales ranging from O(10^{-6} to 10^{0} m), and can contribute to the formation of a convective column of rising air above the fire that drives complex circulations. The characteristics of the updraft within the convective column are most directly related to overall fire intensity but can be modified by meteorological factors such as static stability, background wind speed, background wind shear, and the development of turbulence, and by other fire factors such as fire shape.

Static stability primarily influences the convective column characteristics by affecting the magnitude of the updraft. Higher static stability in the overlying atmosphere will decrease the magnitude of the updraft and lower the equilibrium level. A conditionally unstable atmosphere occurs when the environmental lapse rate is lower than the dry adiabatic lapse rate and is larger than the moist adiabatic lapse rate. When conditionally unstable air becomes saturated, the rising air will have less inhibition, and the magnitude of the updraft increases resulting in a higher equilibrium level.

The background wind profile influences the convective column by advecting heat and moisture released by the fire that contributes to the formation of the convective column. Advection is defined as the transfer of heat or matter by the flow of a fluid. Advection of heat and moisture affects the formation, shape, and location of the convective column. A background wind profile with high wind speeds near the surface can prevent a deep convective column from forming. Background wind profiles with weaker winds near the surface allow a deep convective column to develop in which the air rises until the equilibrium level is reached. Background wind profiles with higher wind speeds near the surface can induce more turbulence within the vicinity of the fire. Turbulence within the vicinity of the fire can affect the characteristics of the convective column and the circulations around it.

The shape of a wildland fire directly impacts circulations in the vicinity of the fire. The shape of the fire induces these circulations as a result of combustion. The warming of air near the surface induces an updraft which requires that air be brought in to replace the rising air. The air being brought in to the fire area is called “inflow”. The characteristics of the inflow can generate vortices along the fire line especially near the edges. The vortices along the fire line can impact fire spread and behavior.

This study investigates the effects of background wind and fire shape on the atmospheric response to a wildland fire. The numerical weather prediction model that is capable of resolving cloud-scale processes, Cloud Model 1 (CM1), is utilized to simulate the atmospheric response to a wildland fire. There are three background wind profiles and three fire shapes for a total of nine simulations that will be analyzed in this study. The results from these nine simulations, when combined with field observations, help improve our understanding of fire-atmosphere interactions.

The thesis will be structured as the following, Chapter I is an introduction to this study. Chapter II is a literature review on both theoretical and observational studies that have examined fire-atmosphere interactions. Chapter III is a description of the methods used and the results of this study. Chapter IV is a discussion and conclusion of this study followed by proposed future work.

CHAPTER II - LITERATURE REVIEW

2.1 Theoretical and Observational Studies

2.1.1 Background Wind

The effect of background wind on fire was first investigated by Byram and Nelson (1951). They used a theoretical approach relating near-surface static stability to turbulence and the formation fire whirls. Byram (1954) focused on the relationship between background wind profiles and fire behavior by looking at a collection of wildland fires and comparing them to the nearest measured wind speed profiles. He categorized the wind profiles that were associated with blowup fires, which are defined as fires that burn with an intensity that seems far out of proportion to apparent burning conditions. The wind profiles Byram observed had negative slopes for the lowest ~5000 ft (~1524 m) with a maximum of 24 miles per hour (10.7 m s^{-1}) at the surface. Only one of his observed soundings had a positive slope for the lowest 1000 m. The conditions that Byram established as those that could cause blowup fires are the following: a free air wind of 18 miles per hour (~8 m s^{-1}) or more at or just above the elevation of the fire, and wind decreasing with height for several thousand feet above the fire with the possible exception of the first few hundred feet. Byram concluded that these atmospheric conditions combined with near surface instability were the reasons for blowup fires.

Rothermel (1972) established the influence of wind on fire spread rates in a laboratory study. Based on wind-tunnel experiments that appeared in Rothermel and Anderson (1966), he derived a relationship for winds and fire spread that depends on wind speed and the slope of topography. The rate of fire spread is determined by raising the relationship between wind speed and fire spread to a fuels component. This relationship established one of the first steady state fire spread rate equations Albini (1982) explored the concepts discussed in Rothermel (1972) and developed a non-linear relationship between wind speed and fire spread rate. Albini (1982) discussed the effects of stronger winds on flame tilting and how that impacts fire spread rates. Albini found that a stronger windspeeds acting on the flames of a wildland fire will increase the fire spread rate.

Steiner (1976) used Byram (1954) as the basis for his study and expanded possible relationship between wind shear and blowup fires. The paper discussed downwind-tilted fire-induced convective column that develops with the background wind increase with height. Steiner argued that tilting enhances the mixing of air on the downwind side of the fire. An excerpt from Steiner et al. (1976) presented in Potter et al. (2012), "... a profile with positive wind shear would produce net divergence on the downwind side of the fire and counteract the surface convergence produced by the fire." While the simulations presented in this study employ a wind profile similar to that which was used in Steiner et al. (1976), net divergence does not develop downwind of the simulated fire. In all of the simulations the surface convergence produced by the fire dominates and is not counteracted by the divergence seen in the simulations.

Potter et al. (2012) focused on many aspects of fire weather research, including the influence of background wind profile and fire shape. The influence of background wind profile was covered at length and was identified as an area that required further investigation. Potter et al. (2012) also suggested that interactions between background wind and temperature profiles control turbulence, mixing and entrainment of rising air in the plume, and influence the conversion of buoyant potential energy to vertical velocity.

2.1.2 Fire Shape

The shape of a wildland fire evolves over multiple spatial and temporal scales. Green et al. (1983) identified three main fire shapes that have been investigated: ovoid shapes (Peet 1967), an ellipsoidal shape (Van Wagner 1969, Anderson 1983, Alexander 1985), and a double ellipsoidal shape (Albini 1976). These shapes have been used in the numerical modeling of wildland fires, although no studies have focused on the effects of fire shape on atmospheric circulations.

The ovoid fire shape model (Peet 1967) relates the head fire and flank fire spread rates by employing an ellipse that comes to a gentle point at one end along the major axis of the ellipse. Although the ovoid fire shape model was found in Green et al. 1983 to be the best representation of wildland fire shapes, it is not used as much as the ellipsoidal fire shape model.

The ellipse fire shape model (Van Wagner 1969) is the most common fire shape studied. Anderson (1983) expanded upon the Van Wagner (1969) ellipsoidal fire shape and related it to wind speed. Alexander (1985) later expanded on the ellipsoidal fire model discussed in Anderson (1983). These studies proposed that the ellipse can be used to describe fire spread under uniform fire conditions and constant atmospheric conditions, where the eccentricity of the ellipse is determined by the background wind speed.

Equations for the double ellipse fire shape model (Albini 1976) were developed for fire spread rates downwind (head fire) and upwind (backing fire). Head fires and backing fires were typically found to have different spread rates for which the ellipsoidal fire shape model cannot account. The double ellipse fire shape model is approximated by two interlocked ellipses across a single axis. The first ellipse models the spread of the backing fire while the second ellipse models the head fire.

2.2 Numerical Studies

2.2.1 Past Numerical Modeling Studies

Computational numerical weather prediction models have been used to study atmospheric phenomenon since the 1950's, but the earliest fire-atmosphere coupled models appeared in the 1990's. Numerical models are ideal for studying fire-atmosphere interactions because collecting the observations necessary to understand the relevant processes occurring during a wildland fire is difficult due to extreme conditions. Fire-atmosphere coupled models have been developed to investigate the relationship between combustion processes at scales ranging from O(10^{-6} to 10^{0} m) and resolvable atmospheric processes at scales ranging from O(10^{1} to 10^{3} m).

One of the first models developed was a two-dimensional fire-atmosphere coupled model presented in Heilman and Fast (1992). Heilman and Fast was one of the first studies to use a numerical model to investigate the hypotheses presented in Byram (1959). Heilman and Fast focused upon the turbulent atmospheric characteristics that result from the sensible heat flux that is associated with a wildland fire. The study documented the development of buoyancy-induced horizontal roll vortices in the vicinity of the simulated fire. The fire was parameterized by applying a constant heat source at the surface with a potential temperature of either 900 or 1500 K. The study employed a model domain with a horizontal extent of 2000 m with 50 m grid spacing. The vertical extent of the model domain was 1800 m with the vertical grid spacing stretched using a log profile (0.27 m at the surface increasing to 190 m grid spacing 100 m AGL and remaining constant above this level). Heilman and Fast (1992) stated: "Results showed a definite effect of wind speed on updraft strength and tilt, as well as roll vortex generation…"; and, "Higher wind speeds produced weaker updrafts, greater tilt, and weaker vortices. The strongest vortices developed when there was no ambient wind."

Clark et al. (1996*b*) was the first study to present a two-way interactive atmosphere-fire coupled model. The study implemented a fire spread parameterization and analyzed the effects of vortices on spread rates within the model. The simulations demonstrated that counter-rotating vortex pairs can result in a phenomenon called “dynamic fingering”. Dynamic fingering occurs when the counter-rotating vortex pairs enhance the winds between them, which can cause the rate of fire spread to increase rapidly.

Linn (1997) documented the development of a fire transport model (FIRETEC). FIRETEC was designed to simulate the behavior of gases and fuels without explicitly resolving the details of the combustion process. FIRETEC was later coupled with an atmospheric dynamics model, HIGRAD (Reisner el. al. 1999, Reisner et al. 2000). The FIRETEC/HIGRAD coupled model has been used to simulate atmosphere-fire interactions over scales ranging from O(10^0 to 10^1 m). The governing equations of this model are based on an approach similar to Reynolds averaging of the Navier-Stokes equations.

A different approach to fire modeling was taken by Mell et al. (2007), which documented the development of an atmosphere-fire coupled model called wildland urban interface (WUI) Fire Dynamics Simulator (WFDS) which was developed from Fire Dynamics Simulator (FDS) (McGrattan et al. 2002). FDS is designed for simulating fires within structures and the combustion of construction type materials. WFDS takes a different approach from other atmosphere-fire coupled models in that it solves the Navier-Stokes equations with an emphasis on low-speed, thermally-driven flows that affect heat and smoke transport. Mell et al. (2007)

focused on fire spread and combustion characteristics of different fuels. Mell et al. (2007) simulated grassland fire experiments that were presented in Cheney et al. (1993) and in Cheney and Gould 1995. The simulations presented found that fires burning under light wind conditions often had more variable fire spread rates and were driven by localized thermal activity.

A LES (Large Eddy Simulation) model approach was documented by Sun et al. (2009). The University of Utah LES model (UU-LES) was designed to study small-scale atmospheric circulations involved in cumulus convection. UU-LES uses a combustion parameterization that is similar to the one employed in Clark et al. (1996b). UU-LES, although simpler than WFDS, compared well with WFDS in the Mell et al. (2007) validation study. Jenkins et al. (2007) used UU-LES to examine the effect of vertical wind shear on the evolution of grassland fires. Jenkins et al. (2007) found that a constant background wind, and a moderate background wind decreasing with height does not promote erratic fire behavior. The simulation that had exhibited the most erratic fire behavior was the simulation that had a tanh-sheared background wind with a surface wind speed of 5 m s^{-1}. This background wind profile was found to influence fire's behavior due to the advection of vorticity by the background wind.

The widely used mesoscale model, the Weather research and Forecasting model (WRF), was coupled with a wildland fire-behavior module named WRF-Fire (Coen et al. 2012). The module is a surface fire behavior model that is coupled with the WRF atmospheric model that allows for the model to simulate fire-atmosphere interactions. The near surface winds from the atmospheric model are interpolated to the finer spatial and temporal resolutions of the fire module. The focus of WRF-Fire is on producing forecasts of fire-spread based on an established mesoscale model. Simpson et al. (2014) used WRF-FIRE to investigate vorticity driven lateral fire spread. The study found that the fire whirls that contribute to the lateral fire spread lead to an increase of the upslope fire spread rate.

Kiefer et al. (2008) used the Advanced Regional Prediction System (ARPS) numerical model (Xue et al. 1991) to simulate the atmospheric response to a wildland fire. ARPS is three-dimensional nonhydrostatic model that was developed from the Miller and White (1984) study. ARPS is a utilized to simulate atmospheric processes on scales ranging from O(10^1 to 10^3 m). In the Kiefer et al. (2008) study, ARPS was configured to use a two-dimensional domain that is 40 km long in the horizontal direction by 10 km high in the vertical. The grid spacing employed horizontally was 50 m and is 40 m on average in the vertical. A soil potential temperature perturbation of 400 K was employed to initiate fire-induced convection in the model. The study investigated the effects of changing the background static stability and wind profiles. The wind profiles used in had a low-level jet feature, and the height of the feature and its effects were the focus of the study.

Kiefer et al. (2009) built on concepts examined in Kiefer et al. (2008) by studying the organization and strength of dry convection using the ARPS model. ARPS was setup similarly to Kiefer et al. (2008), and the study documented that a wind profile with a level of zero wind speed contributed to the formation of new updrafts in a multicellular pattern. The study organized plume characteristics into three different modes labelled: multicell, deep-wave and intense-plume modes, and found that these plume characteristics depended on the background wind profile.

Kiefer et al. (2010) expanded upon these results by employing three-dimensional ARPS simulations to investigate the atmospheric response to a sinusoidal fire shape. The study found that fire lines with large undulations developed areas of convergence upwind of the fire and divergence downwind of the fire. Simpson et al. (2013) used a similar approach to Kiefer et al. (2010) by employing a three-dimensional ARPS simulation to analyze the effects of low-level jets on the convective column produced by a fire. Simpson et al. (2013) identified sensitivities in the downwind convective-plume dynamics to the different background wind profiles from Byram et al. (1954).

2.2.2 Current Numerical Modeling Study

This study uses a high-resolution cloud-resolving model designed to simulate convection, the Cloud Model 1 (CM1) (Bryan and Fritsch 2002). CM1 is a state-of-the-science numerical weather prediction model that is most commonly used to investigate the moist processes associated with atmospheric convection. The model utilizes a method that retains all the terms in the thermodynamic and pressure equations. This allows for CM1's mass errors to be several orders of magnitude smaller than those from other cloud models that integrate pressure equations. Due to this approach CM1 conserves mass and energy better than ARPS and conserves energy better than WRF. One consequence of this approach is the computational requirements of the model. Simulations using moisture take roughly two to three times the wall clock run time than those ran without using moisture.

In Bryan and Fritsch (2002), a case was examined using four different formulations of thermodynamic and pressure equations. The comparison was performed for the same case involving dry and moist convection. The results showed that simulations including additional terms in the governing equations, that would normally be removed due to scale analysis, provided the most accurate results. Due to the complexity in model physics involved with simulating moist air processes, this model is computationally very rigorous. Orf et al. (2017), Coffer et al. (2017), and MacIntosh et al. (2017) have used CM1 to simulate convection associated with severe thunderstorms. To date, no studies have used CM1 to study the atmospheric response to a wildland fire.

CHAPTER III - SENSITIVITIES OF SIMULATED FIRE-INDUCED FLOWS TO FIRE SHAPE AND BACKGROUND WIND PROFILE USING A CLOUD-RESOLVING MODEL

3.1 Introduction

This study uses a numerical weather prediction model to investigate the effects of background wind and fire shape on the atmospheric response to a wildland fire. The numerical weather prediction model that is used is capable of resolving cloud-scale processes, Cloud Model 1 (CM1), is utilized to simulate the atmospheric response to a wildland fire. CM1 will be used to explore the sensitivities of the atmospheric response to a wildland fire to different background wind profiles and fire shapes. Three background wind profiles and three fire shapes for a total of nine simulations, will be analyzed in this study. These sensitivities are explored to understand the atmospheric response to a wildland fire and the possible implications this response has on fire behavior and fire spread. The results from these nine simulations, when combined with field observations, help improve our understanding of fire-atmosphere interactions.

3.2 Methods

3.2.1 Model Setup

The model used in this study is CM1, a three-dimensional, high-resolution, cloud resolving model. The horizontal extent of the domain is 6000 m in both the x and y directions. A uniform horizontal grid spacing of 10 m (600 grid points) and non-uniform vertical grid with an average grid spacing of 40 m (250 grid points) are employed. The domain has a vertical extent of 12500 m. The vertical grid is stretched such that the minimum grid spacing is 2.5 m at the surface and the maximum grid spacing 250 m at the top of the domain. The bottom boundary condition is semi-slip (i.e. partial-slip) with the land use set to the WRF value for grasslands. The roughness length of the surface is set to 0.001 m so as to minimize the effects of friction at the surface. Open-radiative lateral boundary conditions are used, and a Rayleigh damping zone is added to the outermost five grid points at the West/East boundaries to limit the propagation of waves that reach those boundaries. The top boundary condition is open-radiative with a Rayleigh damping zone that starts at 11500 m above the surface extending to the top of the domain at 12500 m. The sponge layer The inverse e-folding time (alpha) for all Rayleigh damping zones is set to $5.0e^{-1}$.

The Smagorinsky turbulent kinetic energy subgrid-scale turbulence closure scheme (Stevens et al. 1999) is used. Surface radiation physics and surface momentum fluxes are turned off. This is done to eliminate any heat, momentum, and moisture fluxes from the land surface. Moisture is turned off in the model, the background atmospheric conditions are without moisture and the fire does not release moisture. Coriolis is turned off because the Coriolis force is negligible at the spatial and temporal scales used in this study. Second order Runge-Kutta time differencing and fifth-order accurate spatial derivatives for the advections terms are employed (Wicker and Skamarock 1998).

3.2.2 Model Simulations

The fire is represented in CM1 by a surface sensible heat flux. The heat flux is zero at the start and linearly increases to 25 Kw m^{-2} in the first ten seconds. The surface sensible heat flux is kept constant through the rest of the simulated period. The magnitude of the sensible heat flux used in this study falls within the range documented in previous modeling studies (Kiefer et al. 2009, 28.8 kW m^{-2}, 15 kW m^{-2}, Heilman and Fast 1992, 37 kW m^{-2}) and compares well with measured data from Clements et al. (2007) (28.5 kW m^{-2}) for a grass fire. The surface fire is located near the center of the domain in to minimize the effects of waves reflecting off the boundaries. Figure 1 shows the three fire shapes that are employed by this study (hereafter, shapes A, B, and, C) that represent a range of curvatures. The total area of each fire shape is the same, as is the west-east cross-section of each fire shape (i.e. each fire is 70 m across from west to east). The magnitude and shape of the sensible heat flux is held constant for the duration of each simulation.

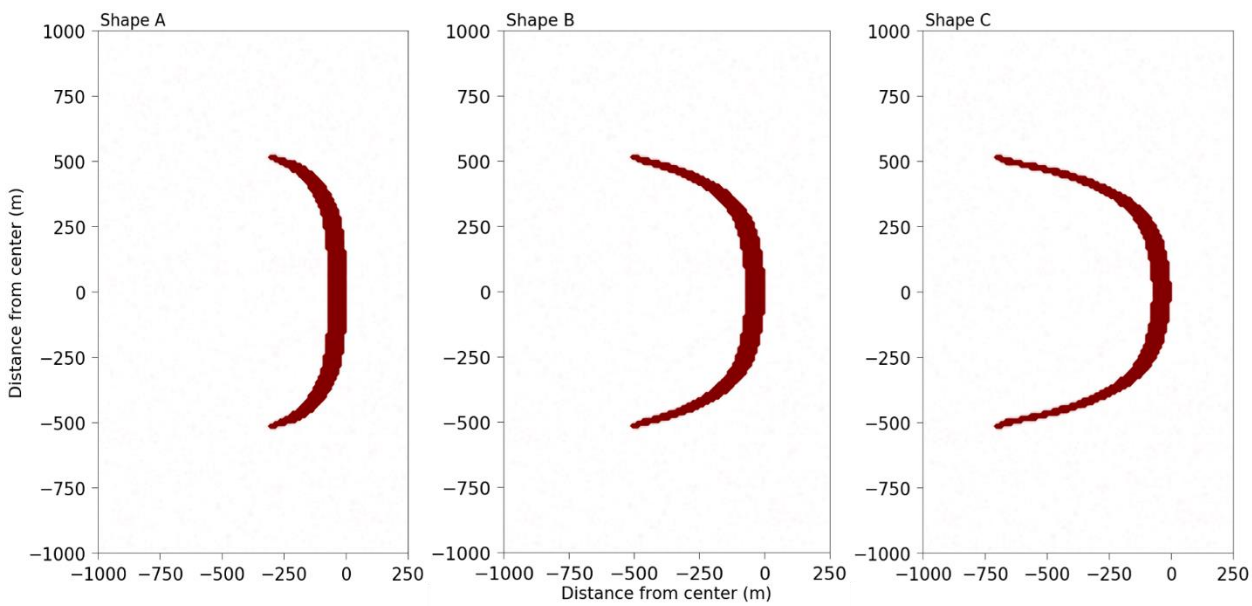

Figure 1. Three fire shapes (shape A, shape B, and shape C) and their location within the model domain. The locations where a sensible heat flux of 25 kW m^{-2} is applied are shaded in red.

Three background wind profiles are used in the simulations (Figure 2). The first wind profile has 0 m s^{-1} background wind speed at all levels. The second and third wind profiles have 5 m s^{-1} and 10 m s^{-1} wind speeds respectively from the top down to 2000 m AGL, decrease linearly to 100 m AGL and then logarithmically to ~0 m s^{-1} at the surface. The three wind profiles used are assumed to be in the positive x-direction. The lowest 100 m of the wind profile features a logarithmic decrease in wind speed from 100 m AGL to the surface. Wind profile 4c in Byram (1954) is similar to the profiles used in this study in that it features a linear increase from 8 miles per hour (~3.5 m s^{-1}) at the surface to 15 miles per hour (~6 m s^{-1}) at a height of 1500 ft above the pilot balloon station, and is held constant above that height. The wind profiles used in this study are assumed to be a positive (westerly) U for all simulations.

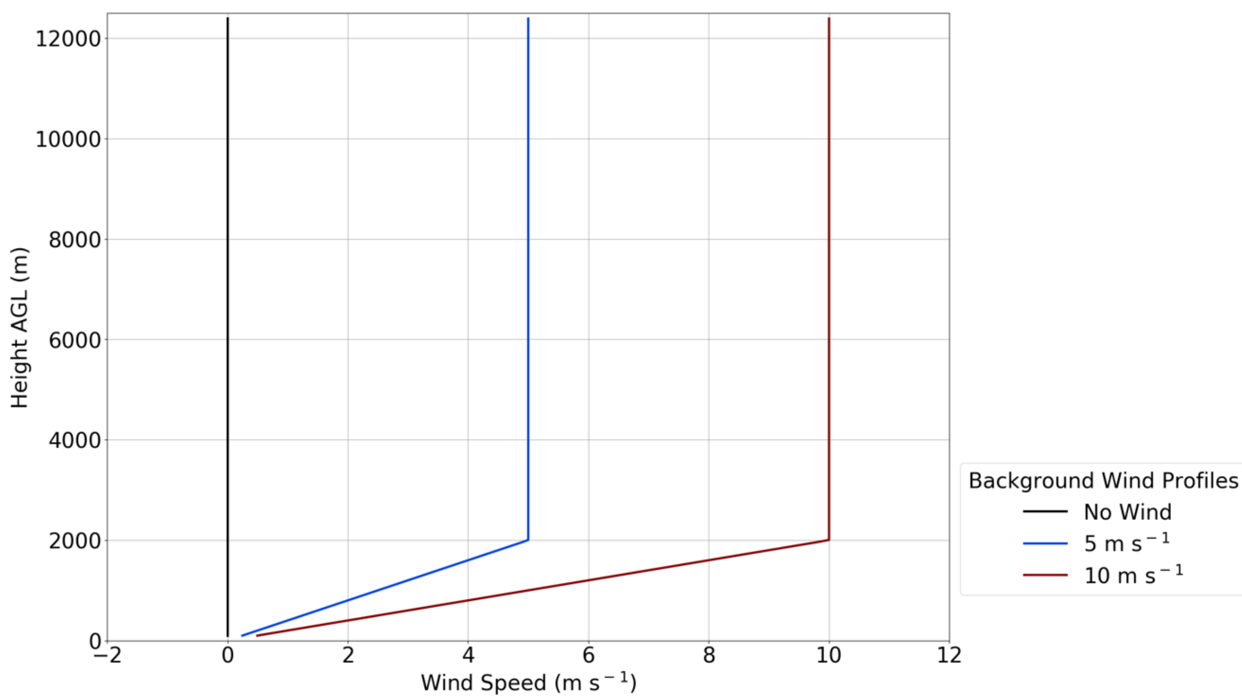

Figure 2. Three background wind profile that are used in the simulations: no background wind (black), 5 m s^{-1} max wind (blue), 10 m s^{-1} max wind (red).

The background temperature profile is assumed to have a moist adiabatic lapse rate for all of the simulations. Table 1 shows all of the simulations that were produced for this study. Each row in the table corresponds to a different background wind profile and each column corresponds to a different fire shape. For simplicity, the first row of table will be referred to as no background wind simulations, the second row as 5 m s^{-1} max wind simulations, and the third row as 10 m s^{-1} max wind simulations. Hereafter individual simulations will be referred by the abbreviations list in the table (e.g. "5shapeB" refers to the simulation with a 5 m s^{-1} max wind profile and fire shape B).

		Background Wind Profile		
		0 m s^{-1}	5 m s^{-1}	10 m s^{-1}
Fire Shape	A	0shapeA	5shapeA	10shapeA
	B	0shapeB	5shapeB	10shapeB
	C	0shapeC	5shapeC	10shapeC

Table 1. All of the simulations analyzed are shown with their respective name and background characteristics.

3.3 Results

3.3.1 Vertical Cross Sections

Figure 3 shows a cross section of u-wind velocity through the center of the model domain 1700 s into all of the simulations. The effect of the differing background wind profiles in the simulations appears as an increase in background wind speed with height in the second and third columns of panels. The effect of the fire on the u-wind is evident in the random, turbulent perturbations that form near the surface at the location of the fire and extend upward over the course of the simulation as a convective column of fire-modified air. The fire-modified air rises until it reaches an equilibrium level (EL) that is determined by the static stability of the background profile of potential temperature, the magnitude of the surface heat flux, turbulent interactions between the perturbation and the background environment, and the background wind. The fire-modified air overshoots the EL and exhibits a vertical oscillation around that level that propagates (asymmetrically) to the left and right in the no background wind simulations and is advected to the right in the simulations with background wind. The fire-modified air overshoots the EL and exhibits a vertical oscillation around that level that propagates (asymmetrically) both up and downwind in the no background wind simulations and is advected downwind in the simulations with background wind. The maximum height of the fire-modified air, as indicated by u-wind perturbations in Figure 3, is lower in simulations with stronger background wind. In the no background wind simulations, the maximum height of fire-modified air at 1700 s decreases from about 1500 m AGL in no background wind simulations (Figure 3, Column 1), to 1250 m AGL in the 5 m s^{-1} max wind simulations (Figure 3, Column 2), and to 1000 m AGL in the 10 m s^{-1} max wind simulations (Figure 3, Column 3). Also note that the magnitude and vertical extent of the negative u-wind perturbations downwind of the fire simulations are larger in simulations with stronger background wind.

The no background wind simulations (Figure 3, Column 1) exhibit negative u-wind upwind of the fire location over a depth of about 750 m. In the 10 m s^{-1} max wind simulations (Figure 3., Column 3), the downwind of the fire u-wind depth is shallower having a depth of about 250 m. Curvature has little influence on the u-wind features directly downwind of the fire, however, it has a large effect on the inflow depths and strength upwind of the fire The near surface u-wind inflow upwind of the fire is lower in depth and smaller in magnitude in simulations with more curvature in the no background wind and 5 m s^{-1} max wind simulations. In the no background wind simulations, the depth of the positive u-wind inflow upwind of the fire is considerably deeper in the 0shapeA simulation (about 500 m) than in the 0shapeC simulation (about 125 m). The magnitude of the inflow is nearly twice as large in the 0shapeC simulation (about 2.9 m s^{-1}) as in the 0shapeA simulation (about 1.5 m s^{-1}). The near surface winds upwind of the fire are stronger with larger background wind for shapes B and C. In the shape C simulations, the maximum inflow upwind is higher in the 0shapeC simulation (approximately 2.9 m s^{-1}) than in the 10shapeC simulation (approximately 1.4 m s^{-1}). The fire induced inflow as large as about 3 m s^{-1} in the no background wind simulations and is as large as about 1 m s^{-1} in the 10 m s^{-1} max wind simulations. The fire induced inflow in the 5 m s^{-1} max wind simulations is as large as 1.5 m s^{-1}.

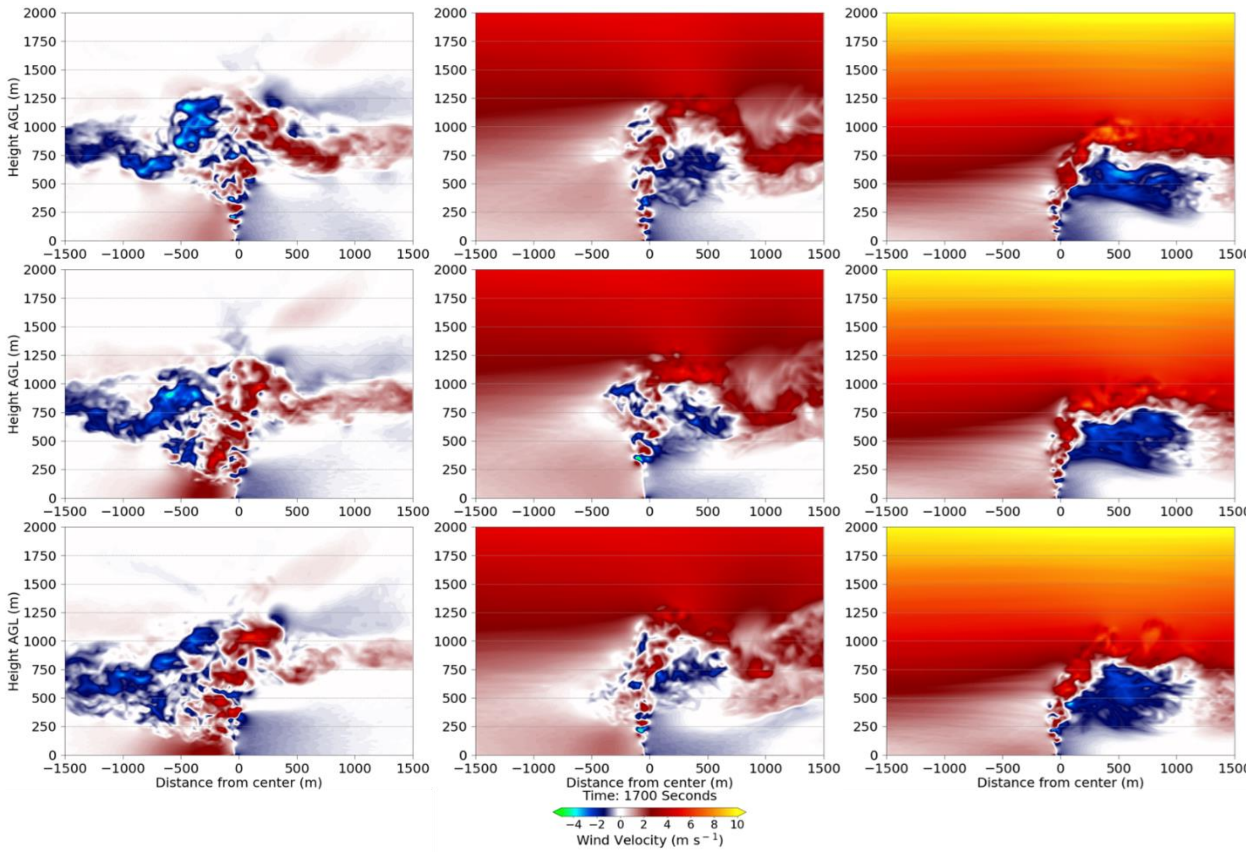

Figure 3. Vertical cross section of u-wind 1700 s into the simulations. u-wind velocities are shaded. Positive values indicate a wind direction to the right, negative values indicate a wind direction to the left.

Vertical velocity is the next topic we examine. Vertical velocity is important to look at to have a better understanding of the characteristics within the convective column. Figure 4 is a cross section of the vertical velocity through the center of the model domain at 1700 s into all of the simulations. The fire-modified air appears as an updraft near the surface, with air rising up to the EL after which the effect of static stability is to produce a vertical oscillation around the EL. Similar to the horizontal wind, the vertical velocity fields are much more sensitive to the background wind profile than to the shape of the fire. The updraft is affected by changes in background wind such that the tilt of the updraft downwind of the fire is steeper in simulations with larger background wind. For the no background wind, the width of the updraft, which is determined by the level with the maximum width of positive vertical velocity values below the EL, increases from 550 m in the 0shapeA simulation to 1020 m in the 0shapeC simulation. In simulations with larger background wind, the width of the updraft is also larger in the shape C simulations than shape A simulations. The width appears to decrease with the increase in wind speed. For example, the 10shapeC simulation has an updraft width of 120 m compared to the 0shapeC simulation, which has an updraft width of 1020 m. For all of the simulations the maximum positive vertical velocities are about 12 m s^{-1}.

In the no background wind simulations (Figure 4, Column 1), there is a larger area of positive vertical velocity below 500 m in simulations with more curvature. In the 0shapeC simulation, the positive vertical velocity values upwind appear approximately 750 m from the center of the domain. In the 0shapeA simulation, the positive vertical velocity values appear upwind approximately 250 m from the center of the domain. Below 500 m AGL, subsidence upwind of the fire is lower in magnitude in no background wind simulations with more curvature. In simulations with a background wind, there is no clear difference in the subsidence upwind. In simulations with a background wind, there is subsidence below 500 m AGL downwind of the fire that appears to decrease in strength with increasing curvature. Subsidence outside of the updraft in the 5shapeA and 5shapeB simulations is weak compared to the no background wind simulations. In the 5shapeC simulation, the magnitude of the subsidence below 500 m AGL is approximately 1 m s^{-1}.

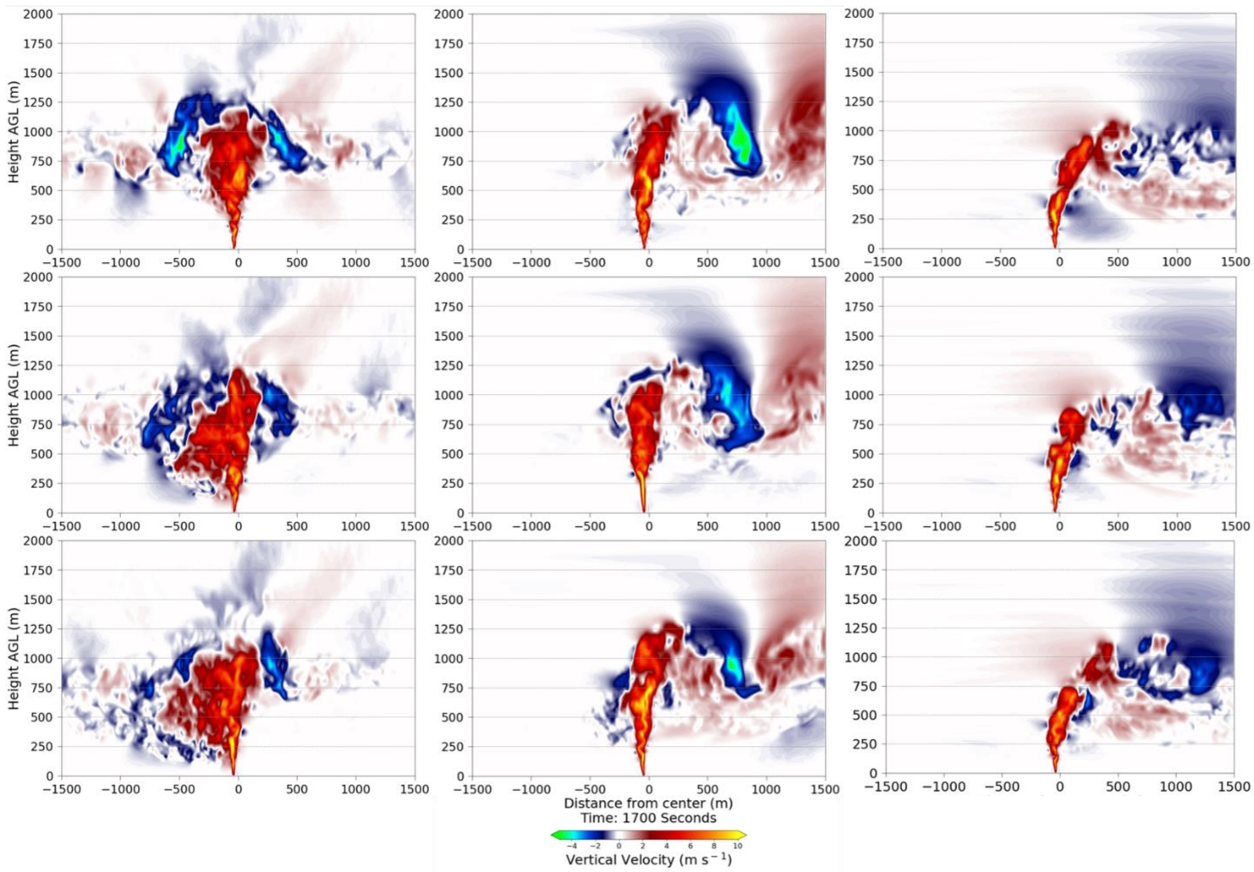

Figure 4. Cross section of vertical velocity 1700 s into the simulations. Vertical velocities are shaded. Positive values indicate an upward wind, negative values indicate a downward wind.

Now we examine the time evolution of the maximum plume height for all of the simulations. Figure 5 is a time series of the maximum plume height for all of the simulations. The maximum plume height is defined subjectively as the maximum height where the vertical velocity is greater than 0.1 m s^{-1}. The maximum plume height in all of the simulations for the first 400 s, after which it oscillates around a characteristic value for each simulation. The maximum plume height in the time series decreases from 2,000 m AGL for the no background wind simulations (Figure 5, Column 1), to 1,475 m AGL for the 5 m s^{-1} max wind simulations (Figure 5, Column 2), and to 1,300 m AGL for the 10 m s^{-1} max wind simulations (Figure 5, Column 3). There is less variation in the maximum plume height over time in the background wind simulations than in the no background wind simulations (compare Figure 5, Columns 2 and 3 to Figure 5, Column 1).

3.3.2 Time Series

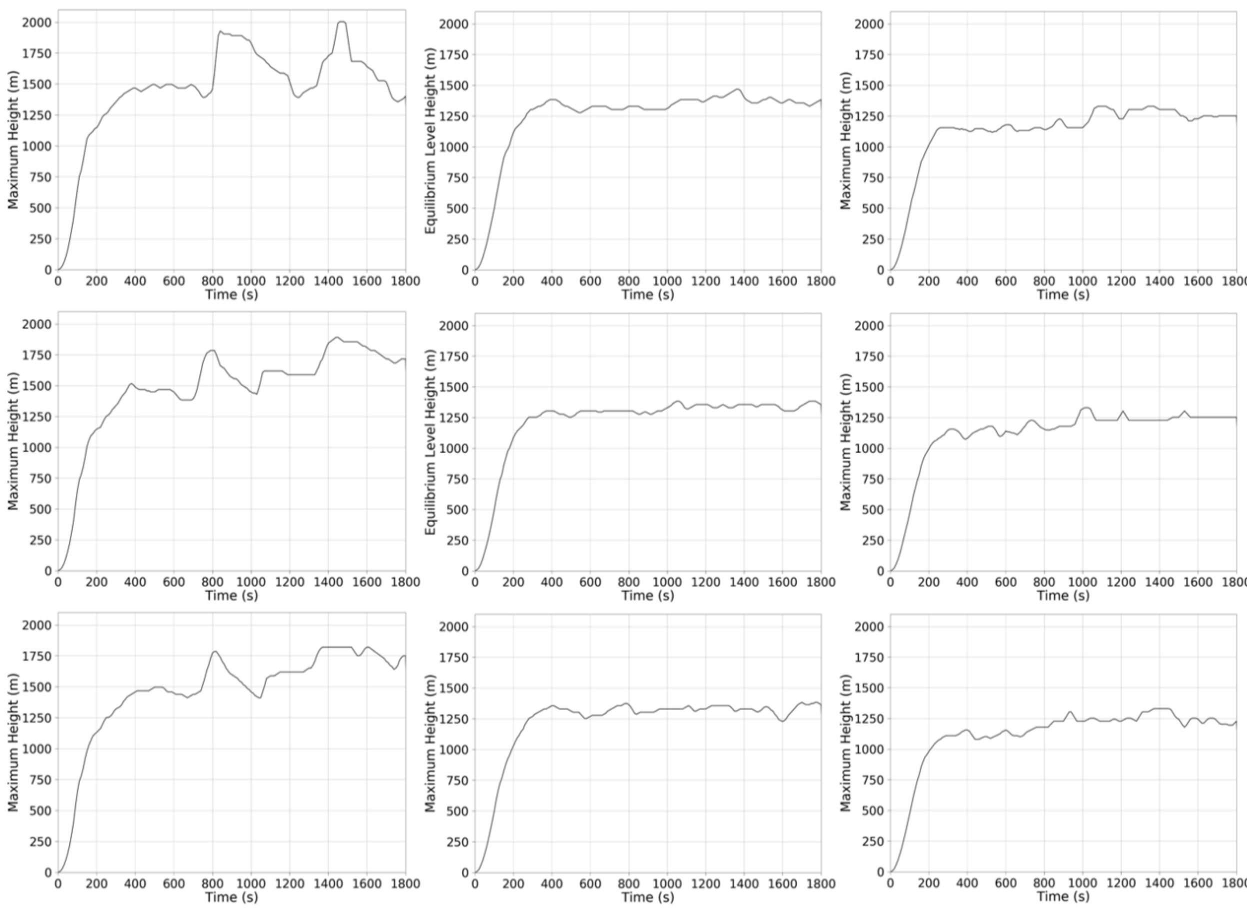

Figure 5. Time series of the maximum plume height for all of the simulations.

3.3.3 Surface Analysis

Next, we examine a surface analysis of perturbations from the background u-wind (Figure 6), which are determined by subtracting the background wind from the u-wind at every grid point in the model domain. The overall pattern for all of the simulations is positive perturbations upwind of the fire and negative perturbations downwind of the fire. The horizontal extent of the inflow upwind of the fire area increases in simulations with increasing background wind and curvature. In the no background wind simulations, the inflow directly upwind of the fire, which has a magnitude of approximately 1.5 – 2 m s^{-1}, is larger with more curvature. In the background wind simulations, the inflow directly upwind of the fire is weaker with magnitudes less than 0.5 m s^{-1}, but the magnitude of the downwind u-wind perturbation is larger compared to no background wind simulations. The maximum magnitude for the downwind u-wind perturbation ranges from approximately -1.0 m s^{-1} in the no background wind simulations to approximately -1.5 m s^{-1} in the 10 m s^{-1} max wind simulations.

In the no background wind and 5 m s^{-1} max wind simulations, a small arc of negative and positive fine-scale perturbations is present along the upper and lower inside flanks of the fire. The fine-scale perturbations have a larger horizontal extent in simulations with more curvature. The fine-scale perturbations have a smaller horizontal extent in simulations with larger background wind. In the 10 m s^{-1} max wind simulations, areas of negative u-wind downwind of the fire extend horizontally orthogonal to the curvature of the fire. The areas of negative u-wind downwind of the fire form 250 m further upstream with each increase in curvature.

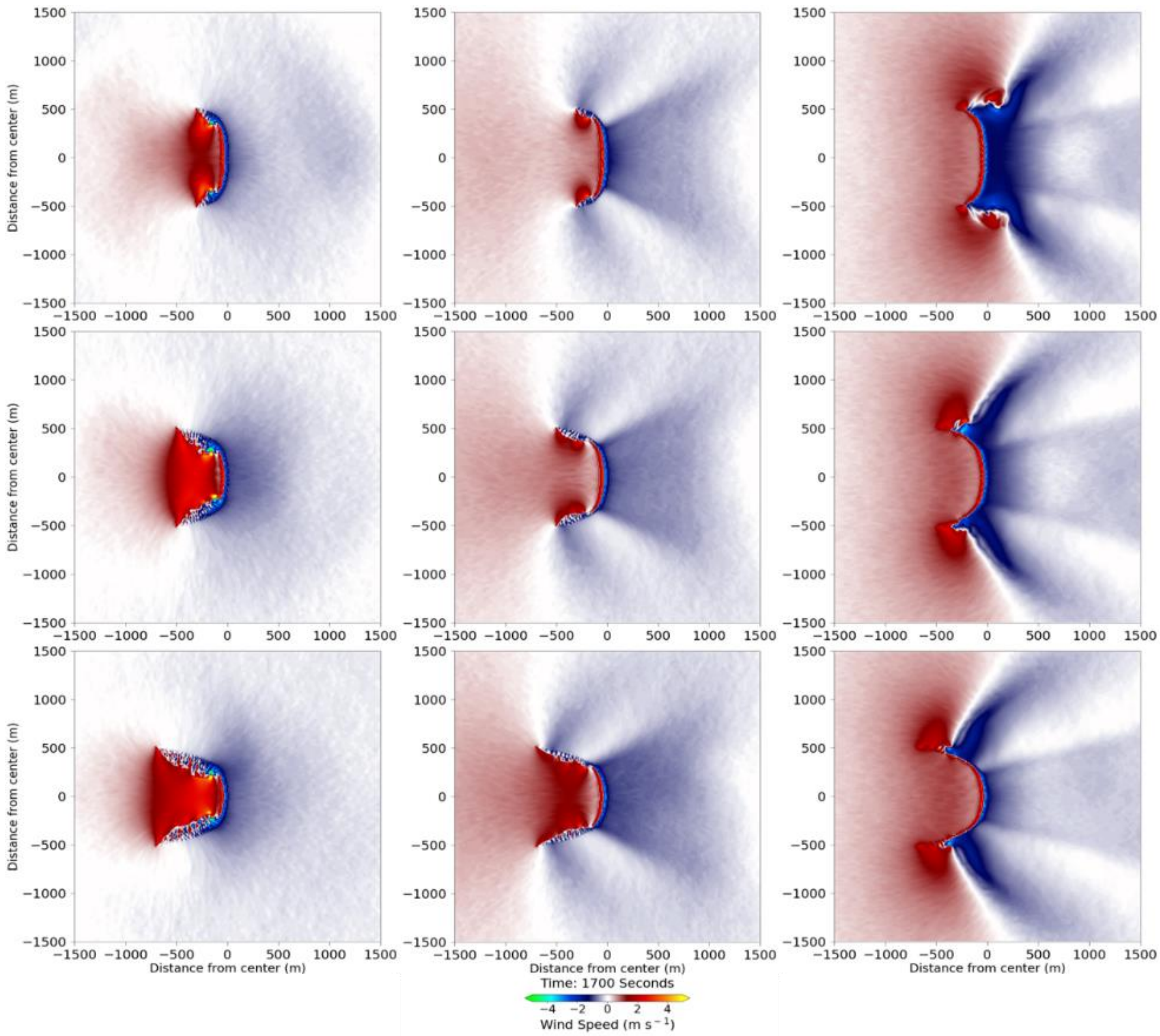

Figure 6. Horizontal cross section of perturbations from background u-wind at the surface 1700 s into the simulations. The perturbations of u-wind at the surface are shaded. Positive values indicate a perturbation wind direction to the right, negative values indicate a perturbation wind direction to the left.

A surface analysis of divergence 1700 s into the simulations is examined next (Figure 7). Divergence/convergence is defined as the net horizontal outflow/inflow of air at any given point. There is convergence inside the fire area and divergence directly outside of the fire area. The magnitude of the divergence directly upwind of the fire is larger with more curvature in the no background wind (Figure 7, Column 1) and 5 m s^{-1} max wind simulations (Figure 7, Column 2). The magnitude of the divergence directly upwind of the fire area is approximately -2.0 s^{-1} in the no background wind simulations and approximately zero s^{-1} in the background wind simulations. Curvature has no clear influence on the divergence directly upwind of the fire in the 10 m s^{-1} max wind simulations (Figure 7, Column 3).

Simulations with background wind develop linear convergence features ("streamers") of magnitude approximately -0.25 s^{-1} that coincide with the patterns in u-wind perturbations downwind of the fire (Figure 6). The magnitude of the streamers in the 10 m s^{-1} max wind simulations is approximately 0.25 s^{-1} and have a length of approximately 1,500 m. The streamers are shorter in the 5 m s^{-1} max wind simulations (approximately 1,000 m) than in the 10 m s^{-1} max wind simulations. There are areas of alternating convergence and divergence in the 10 m s^{-1} max wind simulations.

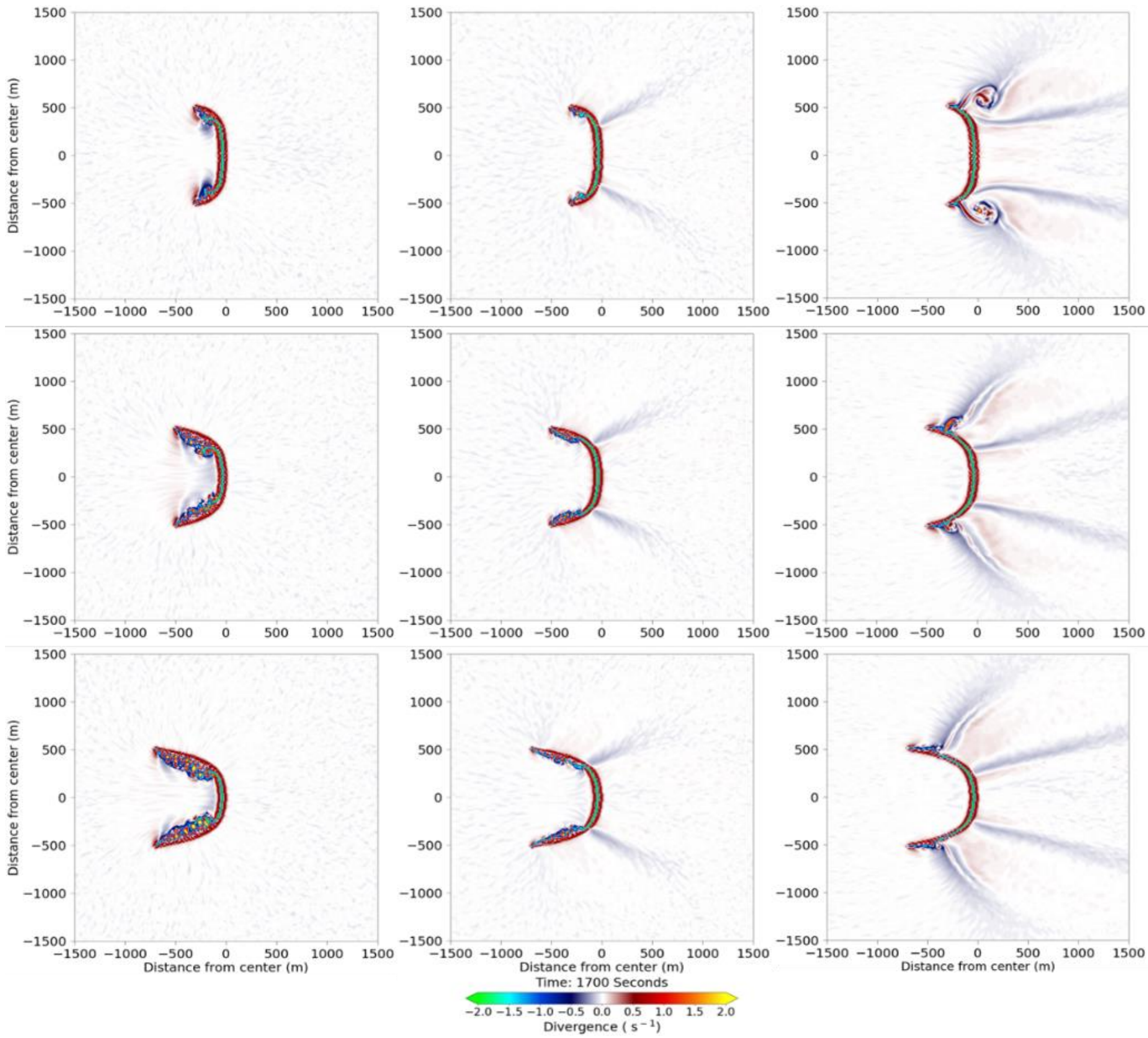

Figure 7. Horizontal cross section of divergence at the surface 1700 s into all of the simulations. Divergence is shaded by positive values, convergence is shaded by negative values.

3.3.4 Vertical Vorticity

We turn our attention to vertical vorticity which is important for fire spread implications. The focus will be on vertical vorticity since it is the dominant component of the fire induced vorticity. Figure 8 is a time series of the distribution of vertical vorticity for all of the simulations. Vertical vorticity is defined as the instantaneous spin around the z-axis of air at a given point. Positive vertical vorticity indicates cyclonic (counter-clockwise) rotation, whereas, negative vertical vorticity indicates anti-cyclonic (clockwise) rotation. Figure 8 shows the vertical vorticity values separated into positive and negative distributions, with the 25th percentile, mean, 95th percentile and min/max of each distribution. Only values greater/less than +/- 0.25 s^{-1} are shown. The 5 m s^{-1} max wind simulations show the least variation over time in the min/max and 95th percentile values, and it also show the least sensitivity to curvature. The min/max vertical vorticity in the no background wind simulations reach values of approximately +/- 1.25 s^{-1} and exhibit more variability over time than the background wind simulations. In the 5 m s^{-1} max wind simulations (Figure 8, Column 1), 5shapeA and 5shapeB have smaller min/max vertical vorticity (approximately +/- 0.75 s^{-1}) than the no background wind simulations. In the 10 m s^{-1} max wind simulations, 10shapeA has the strongest min/max vertical vorticity (approximately +/- 1.0 s^{-1}), whereas 10shapeC has the weakest min/max vertical vorticity (approximately +/- 0.7 s^{-1}) and varies the least over time.

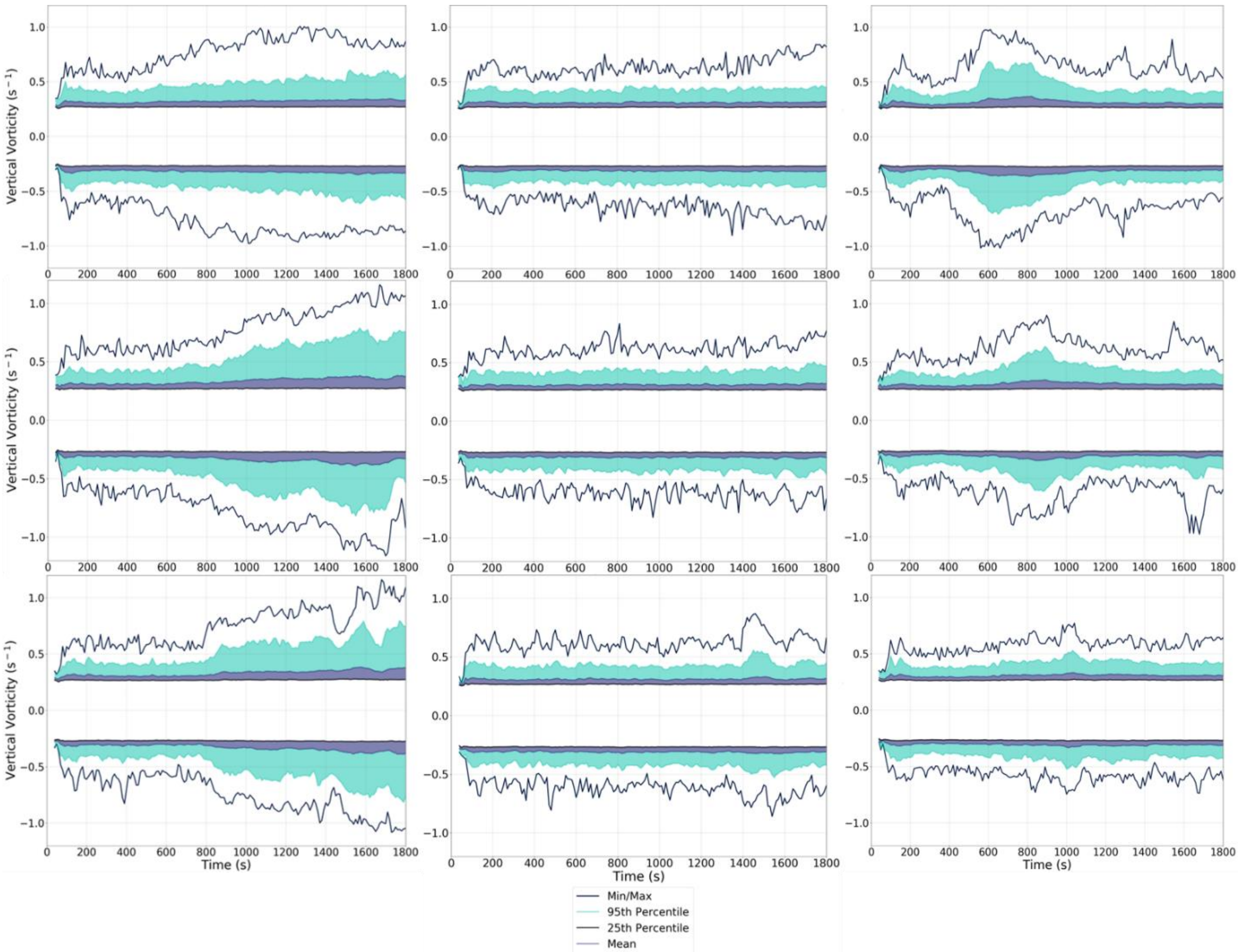

Figure 8. Timeseries of domain wide vertical vorticity distributions. The vertical vorticity values greater/less than +/- 0.25 s^{-1} are analyzed in the distribution. The min/max (dark blue), 95th percentile (shaded teal), 25th percentile (black), and mean (shaded purple).

Figure 9 is a surface analysis of vertical vorticity 1700 s into all of the simulations. The overall pattern indicates the fire location and the significant differences in vertical vorticity patterns that develop in each of the simulations due to the effects of background wind and curvature.

In the no background wind simulations (Figure 9, Column 1), areas of higher magnitude vertical vorticity develop upwind of the fire along the flanks in the interior arc. Fine-scale vertical vorticity perturbations develop upwind of the fire, and these perturbations cover a larger area in simulations with more curvature. The vertical vorticity features that form along the fire arc have the opposite sign (negative) of the largest magnitude vertical vorticity features (positive) that form upwind along the flanks in the interior of the fire.

In the 5 m s^{-1} max wind simulations (Figure 9, Column 2), areas of higher magnitude vertical vorticity also form upwind of the fire along the flanks in the interior of the arc. The maximum positive/negative vertical vorticity magnitudes are weaker in the 5 m s^{-1} max wind simulations (approximately +/- 0.6 s^{-1}) than in the no background wind simulations (approximately +/- 1.0 s^{-1}). These maximum positive/negative magnitudes of the vertical vorticity are located farther upwind in simulations with less curvature. The number of individual vortices is also larger in simulations with more curvature. Fine-scale vertical vorticity perturbations are directly upwind of the fire. These fine-scale vertical vorticity perturbations increase in area with more curvature. The sign of the fine-scale vertical vorticity perturbations varies more in the 5 m s^{-1} max wind simulations than in the simulations with no background wind.

In the 10 m s^{-1} max wind simulations (Figure 9, Column 3), areas of higher magnitude vertical vorticity do not develop upwind of the fire, but instead develop downwind. The distance between the outside flanks of the fire and these areas of higher magnitude vertical vorticity is larger in simulations with more curvature. The maximum positive/negative magnitudes of the vertical vorticity in the 10 m s^{-1} max wind simulations are approximately +/- 0.5 s^{-1}. The location of the maximum positive/negative magnitudes of vertical vorticity are more upwind with more curvature. The sign of the higher magnitude vertical vorticity areas, in the 10 m s^{-1} max wind simulations, are the opposite of the same areas that develop in the no background wind and 5 m s^{-1} max wind simulations. The fine scale perturbations in the fire are also the opposite sign of the higher magnitude vertical vorticity values. The sign of these fine-scale vertical vorticity perturbations (positive) is the opposite of that seen in the no background wind simulations (negative). These results suggest that stronger background wind contributes to a reversal in the sign of the maximum vorticity in the vicinity of the fire.

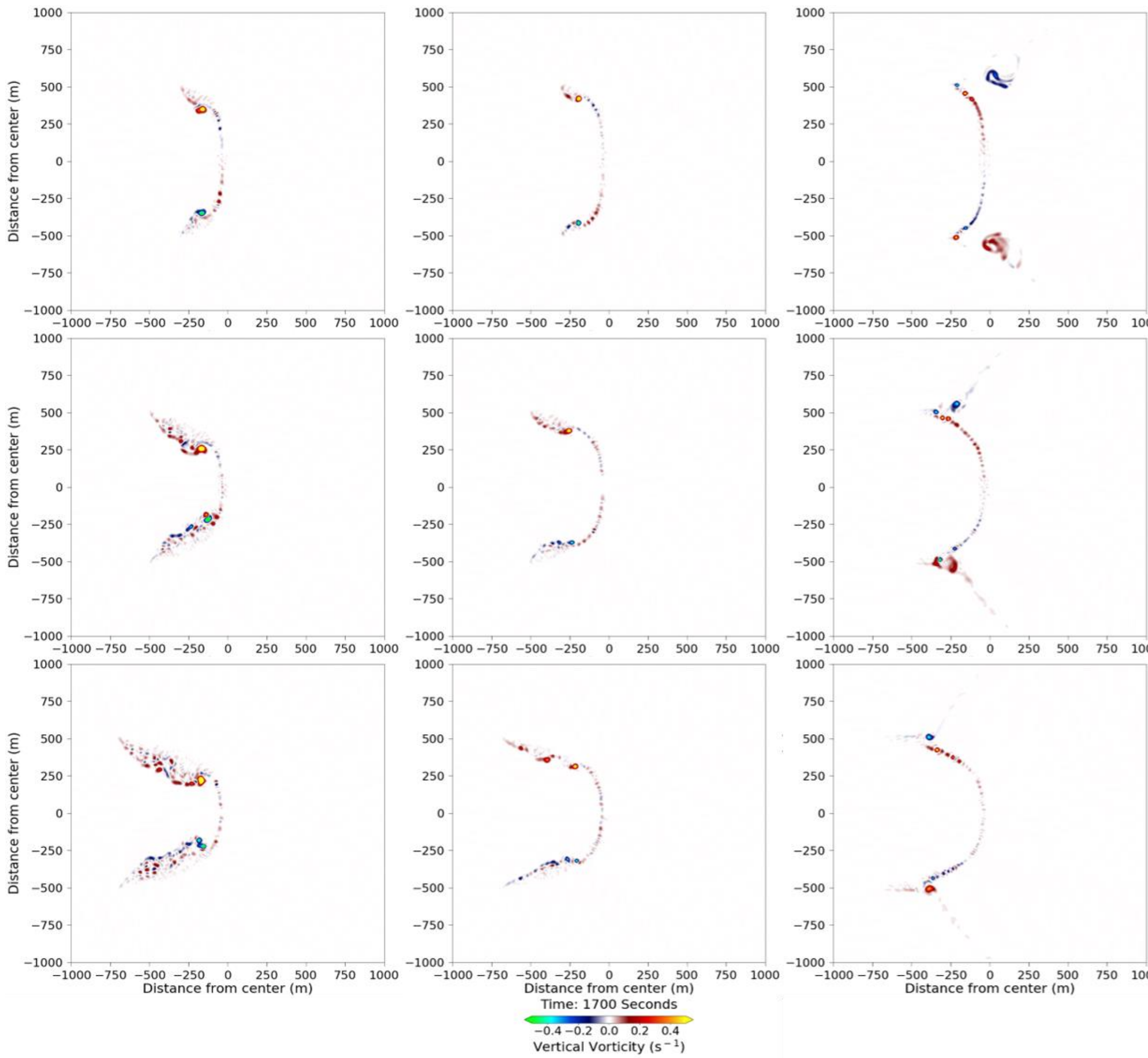

Figure 9. Horizontal cross section of vertical vorticity at the surface 1700 s into all of the simulations. Positive values of vertical vorticity indicate cyclonic rotation, and negative values of vertical vorticity indicate anticyclonic rotation.

CHAPTER IV - DISCUSSION AND CONCLUSION

This study examines the atmospheric response to a wildland fire using the CM1 numerical weather prediction model. CM1 is used to produce nine simulations with three different fire shapes and three different background wind profiles. The results demonstrate that CM1 is capable of simulating the atmospheric response to a wildland fire, and that the response is sensitive to background wind profiles and fire shape. While all the meteorological variables analyzed in this study showed some sensitivity, the degree of sensitivity varies depending on the meteorological variable that is considered. Vertical vorticity is found to exhibit the greatest sensitivity to both fire shape and background wind profile.

The background wind profile affects the tilt of the convective column, contributing to a downwind tilt that is stronger in simulations with a stronger maximum background wind speed. This result agrees with Heilman and Fast (1992), but it also establishes that strong surface winds are not necessary for producing a convective column that tilts downwind. While the simulations presented in this study employ a wind profile similar to that which was used in Steiner et al. (1976), net divergence does not develop downwind of the simulated fire. In all of the simulations the surface convergence produced by the fire dominates and is not counteracted by the divergence seen in the simulations.

The overall distribution of the simulated horizontal and vertical velocities is less sensitive to fire shape than to the background wind profile. The maximum plume height is more sensitive to background wind than fire shape. In the no background wind simulations, the highest maximum plume heights were lower in simulations with stronger background winds. Surface divergence is more sensitive to background wind then fire shape. In simulations with background wind, streamers of convergence form downwind of the fire and are longer in the 10 m s^{-1} maximum wind simulations.

The simulated vertical vorticity features exhibit the most differences in the simulations and are driven by changes in both background wind and fire shape. The vorticity features form in different locations, have different magnitudes, and different distributions in each of the simulations. In the no background wind simulations and the 5 m s^{-1} maximum wind simulations, fine-scale perturbations form, upwind of the fire along the flanks in the interior of the arc. The fine scale vertical vorticity perturbations that form along the interior flanks of the fire arc have the opposite sign of the largest magnitude vertical vorticity features that form upwind. The highest magnitude vertical vorticity values form in the simulations with no background wind, which agrees with the results of Heilman and Fast (1992). Increasing background wind speed lowers the magnitude of the minimum/maximum vertical vorticity values. In the 10 m s^{-1} max wind simulations, maximum values of both positive and negative vertical vorticity form farther upwind with more curvature. The fine scale perturbations in the fire are the opposite sign of the highest magnitude vertical vorticity features. The sign of these fine-scale vertical vorticity perturbations (positive) is the opposite of that in the no background wind simulations (negative). These results suggest that stronger background wind contributes to a reversal in the sign of the maximum vorticity in the vicinity of the fire. This result could have implications for both fire fighter safety and for understanding fire spread.

The limitations of this study start with the idealized horizontally homogenous atmospheric background conditions. A linearly increasing potential temperature profile is used for background temperature distribution, but in reality, atmospheric stratification could be more stable or unstable. The background wind profiles used, which increases logarithmically from surface to 100 m, linearly from 100 to 2000 m and remains constant until model top, is also highly idealized. A real atmosphere can be characterized by multiple layers with different wind speed and wind shears. An even bigger limitation is the lack of moisture both in the background atmospheric condition and release from fire combustion. Last, but not least, the fire is introduced in the model by a surface sensible heat flux that is homogenous in the fire zone and static, but in reality, fire intensity can change due to heterogeneity in fuels, changes in atmospheric conditions, and fire-atmosphere interactions.

The next steps for this study are to expand on the sensitivities presented here. Using fire observations and combining them with future simulations could be useful in determining how close, or far, from reality the model results are when simulating wildland fires. In addition to combining simulation and observational data, exploring different fire shapes and additional background wind profiles could be a way to expand on topics covered in this study. Due to the threshold behavior exhibited in the vertical vorticity, background wind profiles between 5 m s^{-1} and 10 m s^{-1} should be examined. The effects of moisture, interactive fire parameterizations, and forest overstory could be examined. The ultimate goal of CM1 simulations of wildland fires is to explore the effects and sensitives to moisture of pyrocumulus, pyrocumulonimbus, and deep convective circulations.

APPENDIX

Appendix

The following section will show figures from the simulations presented in this study. The figures below will present surface u-wind, surface divergence, and surface z-vorticity 600 and 1200 s into all of the simulations. Lastly, three-panel plots of x-vorticity, y-vorticity, and v-winds will be shown at 600, 1200, 1700 s in each simulation.

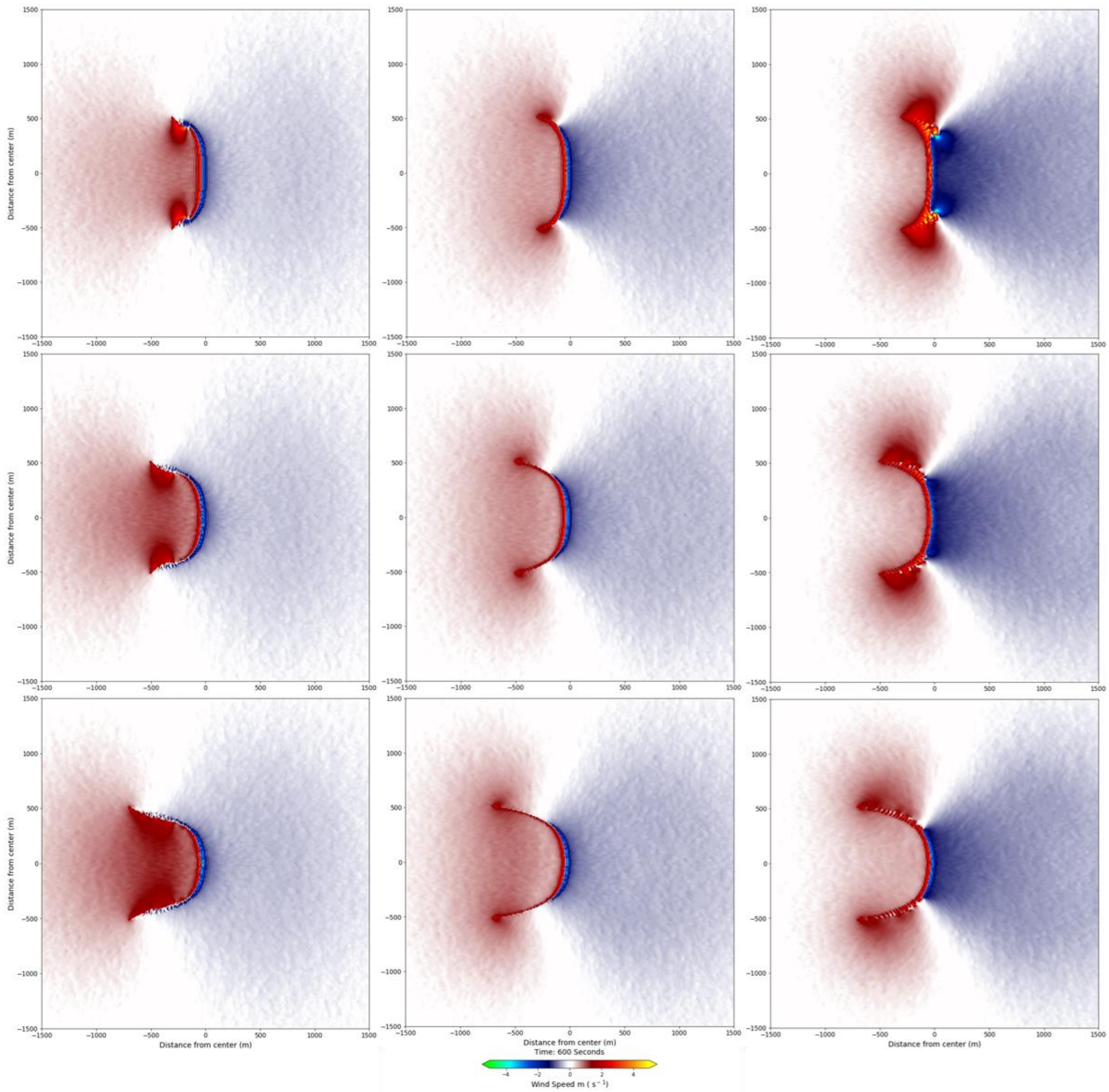

Figure A1. Horizontal cross section of the perturbation of u-winds at the surface 600 s into the simulations. The perturbation of u-winds at the surface are shaded. Positive values indicate a wind direction to the right, negative values indicate a wind direction to the left.

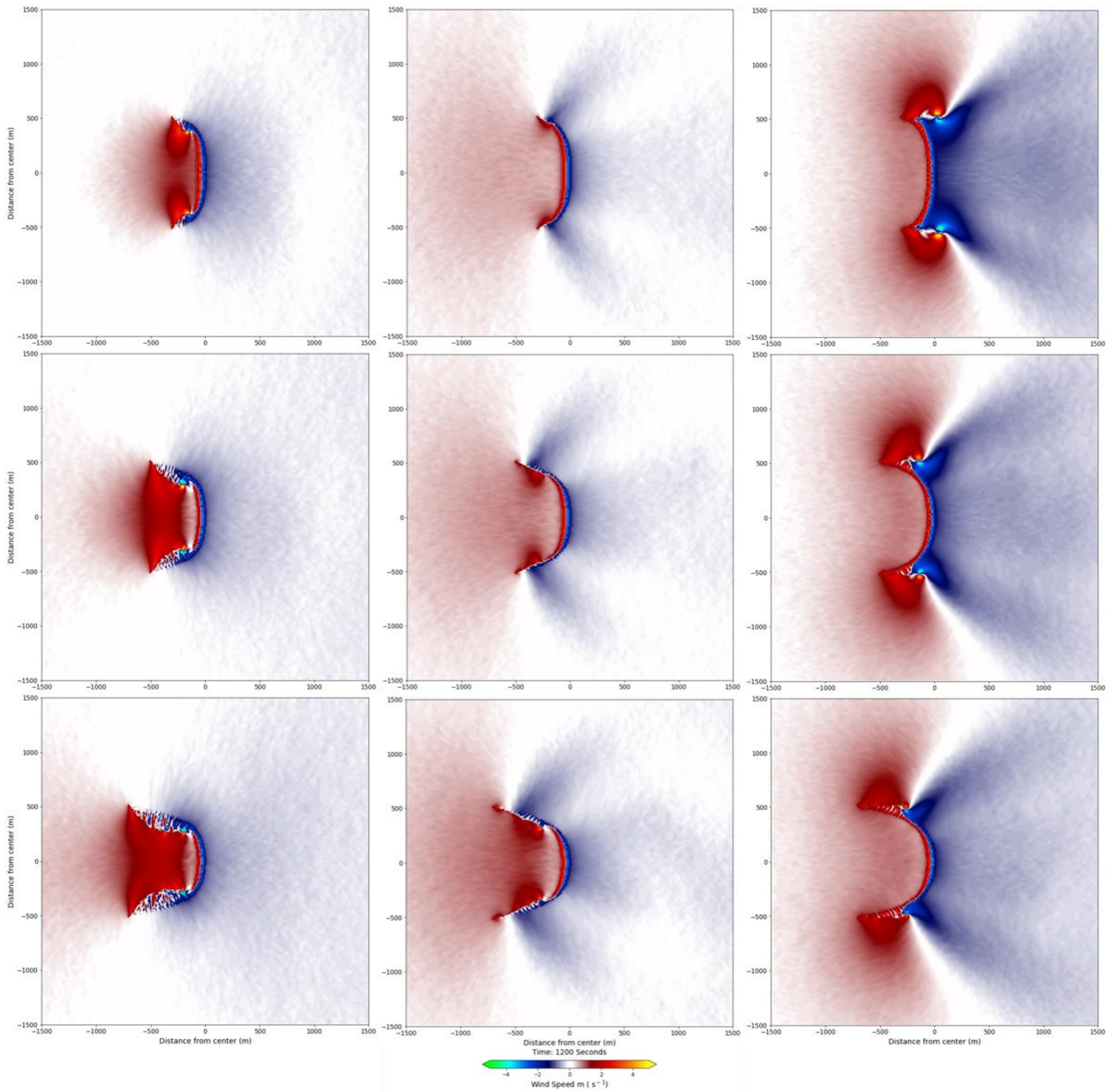

Figure A2. Horizontal cross section of the perturbation of u-wind at the surface 1200 s into the simulations. The perturbation of u-wind at the surface are shaded. Positive values indicate a wind direction to the right, negative values indicate a wind direction to the left.

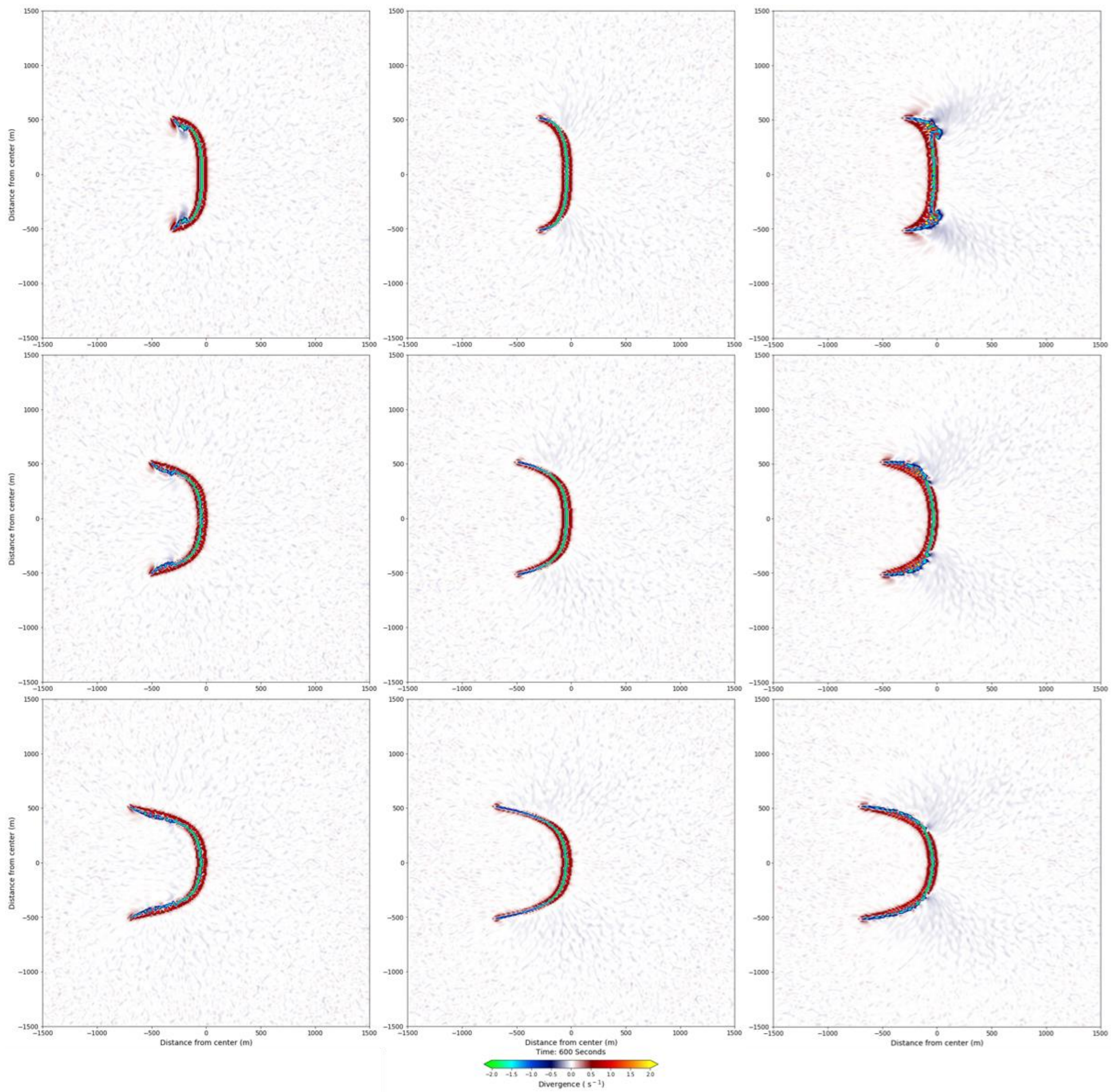

Figure A3. Horizontal cross section of divergence at the surface 600 s into the simulations.

Divergence is shaded by positive values, convergence is shaded by negative values.

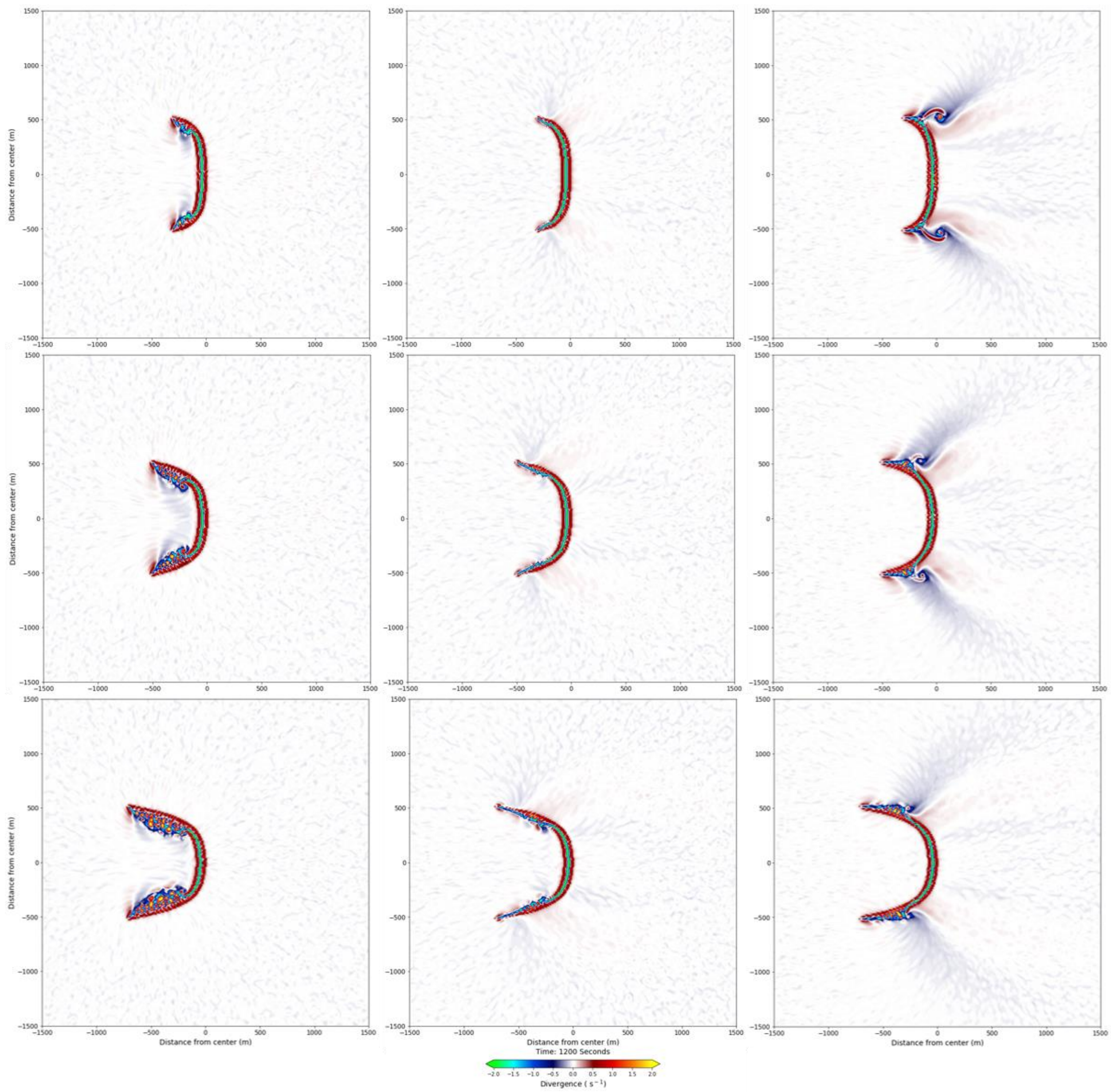

Figure A4. Horizontal cross section of divergence at the surface 1200 s into the simulations.

Divergence is shaded by positive values, convergence is shaded by negative values.

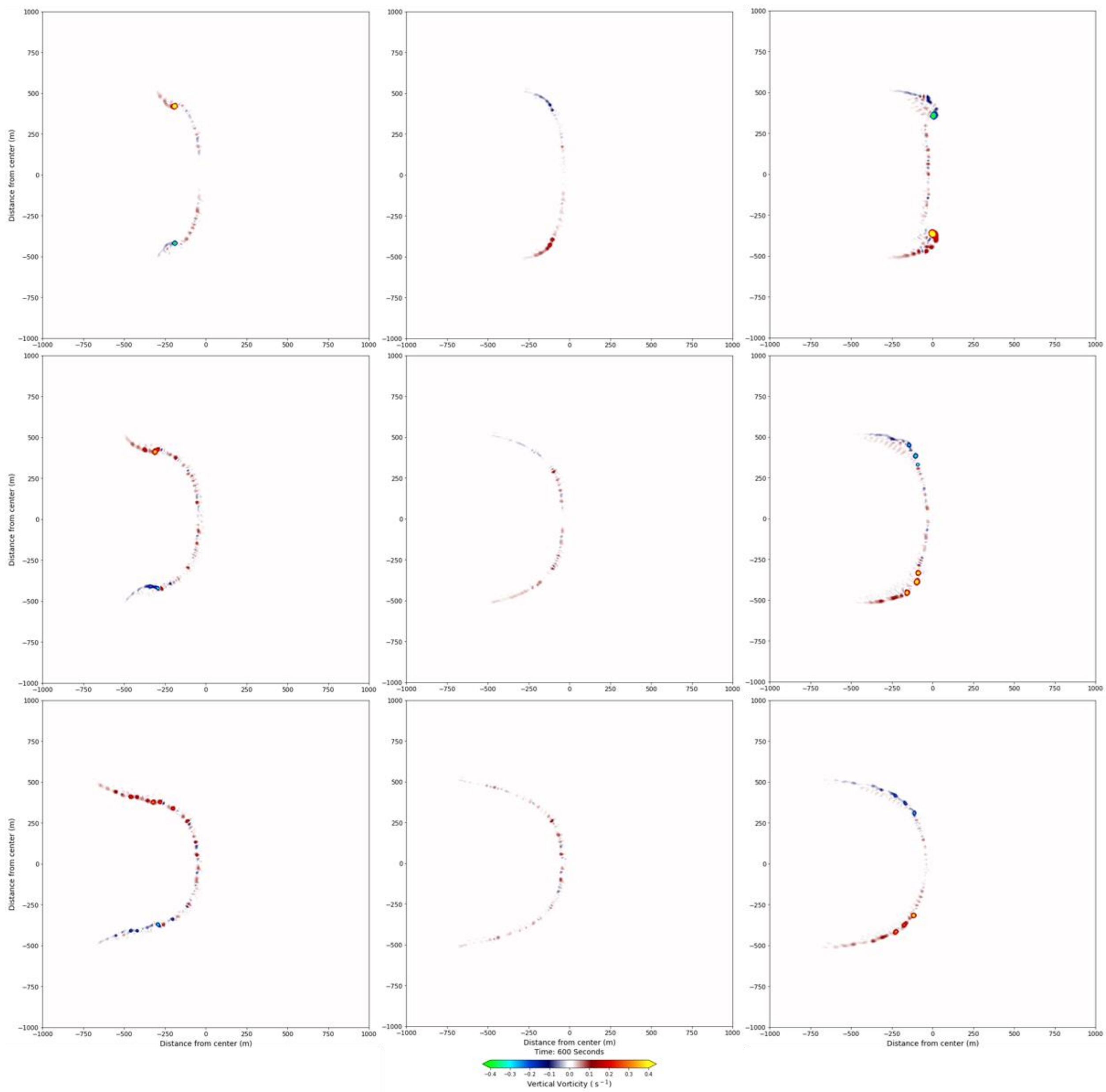

Figure A5. Horizontal cross section of vertical vorticity at the surface 600 s into the simulations. Positive values of vertical vorticity indicate cyclonic rotation, and negative values of vertical vorticity indicate anticyclonic rotation**.**

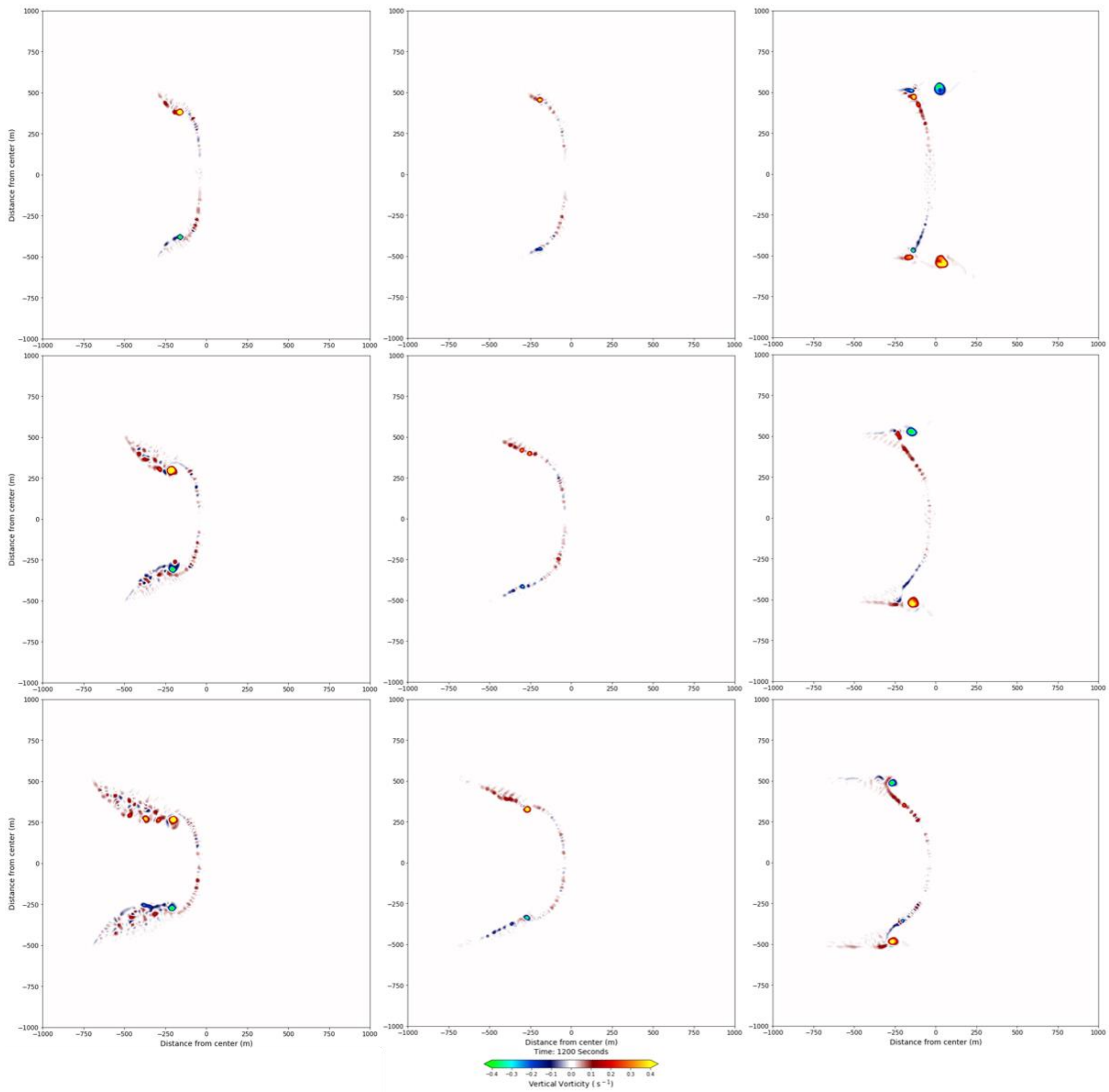

Figure A6. Horizontal cross section of vertical vorticity at the surface 1200 s into the simulations. Positive values of vertical vorticity indicate cyclonic rotation, and negative values of vertical vorticity indicate anticyclonic rotation**.**

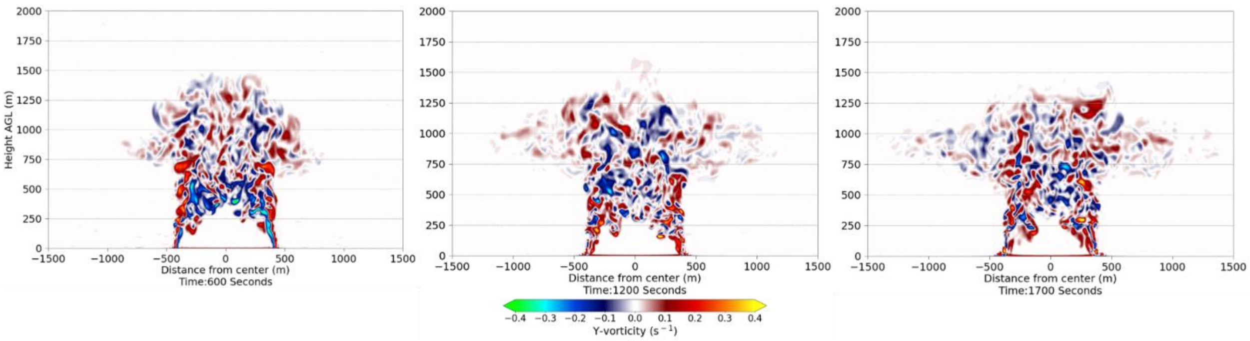

Figure A7. Vertical cross section of y-vorticity at x = 285 (150 m upwind of the front of the fire). The y component of vorticity for the 0ShapeA simulation is shaded such that positive values of y-vorticity indicate cyclonic rotation about the y-axis, and negative values of y-vorticity indicate anticyclonic rotation about the y-axis.

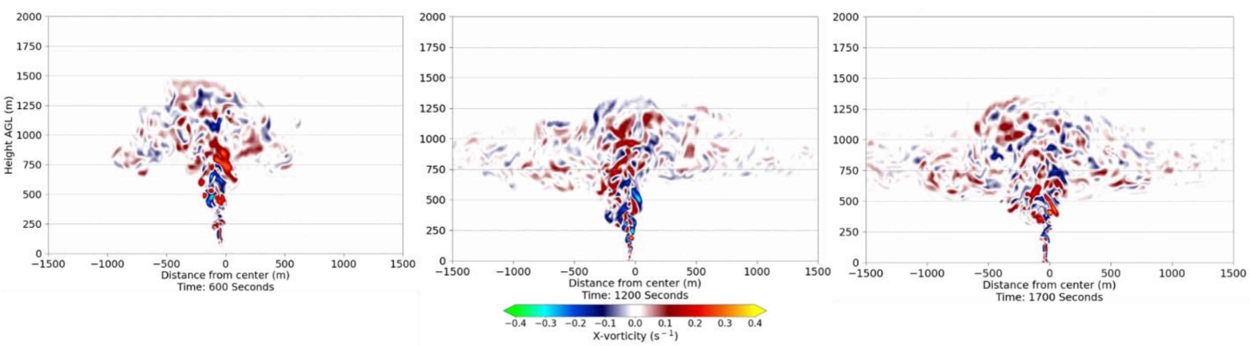

Figure A8. Vertical cross section of x-vorticity through the center of the domain. The x component of vorticity for the 0ShapeA simulation is shaded such that positive values of x-vorticity indicate cyclonic rotation about the x-axis, and negative values of x-vorticity indicate anticyclonic rotation about the x-axis.

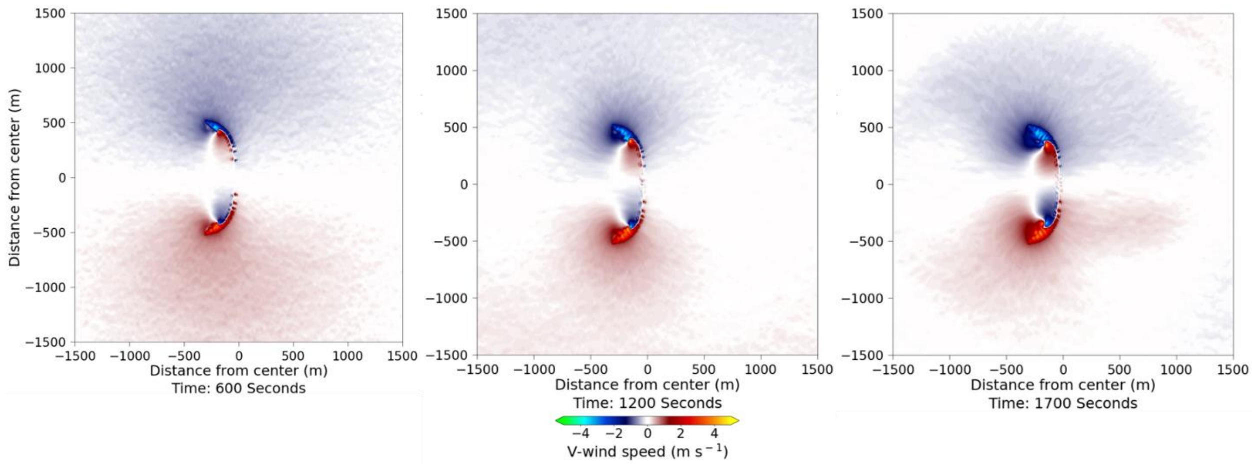

Figure A9. Horizontal cross section of the v-winds at the surface 600, 1200, 1700 s respectively into the 0ShapeA simulation. The v-winds at the surface are shaded. Positive values indicate a wind direction from the bottom to the top of the image, negative values indicate a wind direction from the top to the bottom of the image. Convergence of the winds inside the fire arc is associated with the same location of the vertical vorticity minimum/maximum features.

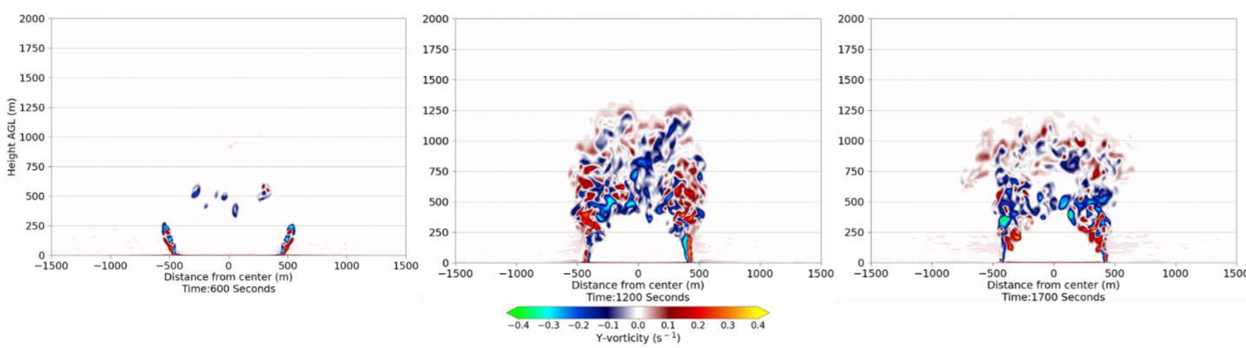

Figure A10. Vertical cross section of y-vorticity at x = 285 (150 m upwind of the front of the fire). The y component of vorticity for the 5ShapeA simulation is shaded such that positive values of y-vorticity indicate cyclonic rotation about the y-axis, and negative values of y-vorticity indicate anticyclonic rotation about the y-axis.

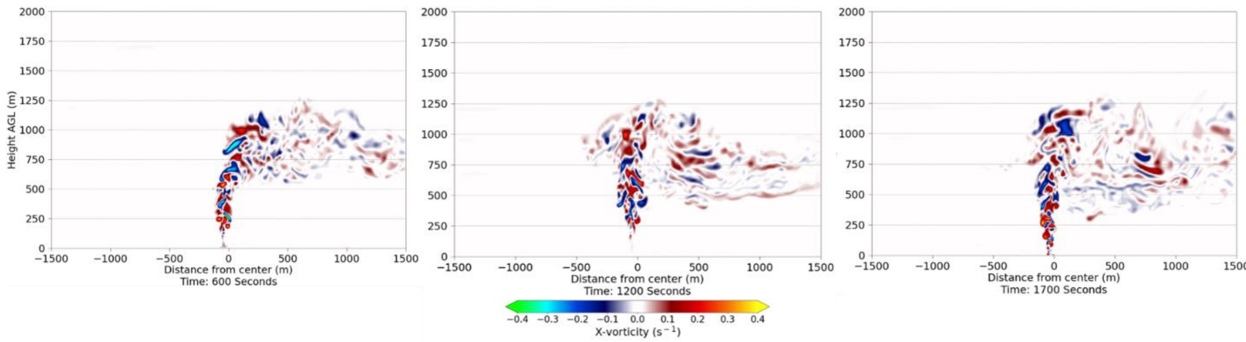

Figure A11. Vertical cross section of x-vorticity through the center of the domain. The x component of vorticity for the 5ShapeA simulation is shaded such that positive values of x-vorticity indicate cyclonic rotation about the x-axis, and negative values of x-vorticity indicate anticyclonic rotation about the x-axis.

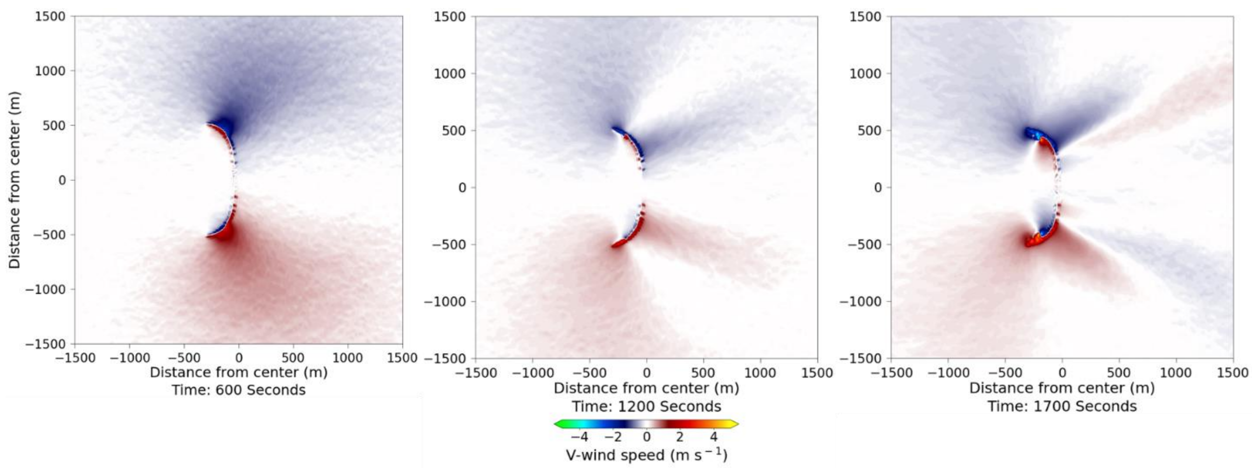

Figure A12. Horizontal cross section of the v-winds at the surface 600, 1200, 1700 s respectively into the 5ShapeA simulation. The v-winds at the surface are shaded. Positive values indicate a wind direction from the bottom to the top of the image, negative values indicate a wind direction from the top to the bottom of the image. Convergence of the winds inside the fire arc is associated with the same location of the vertical vorticity minimum/maximum features.

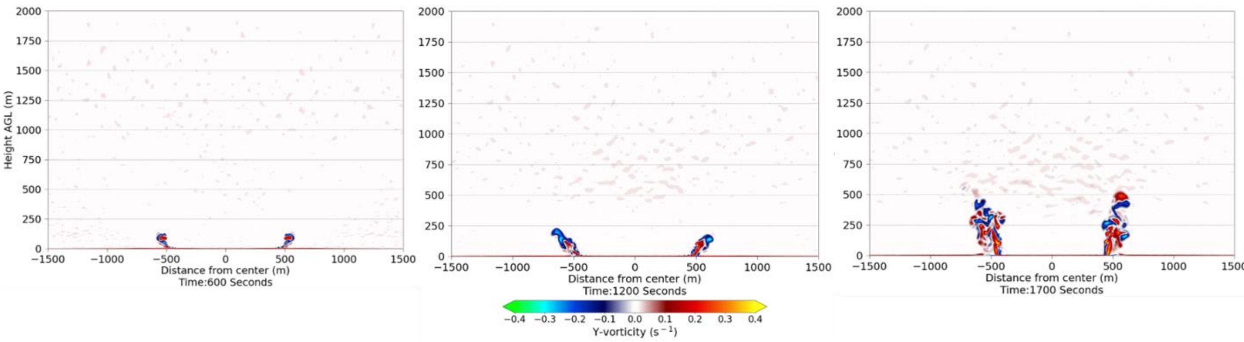

Figure A13. Vertical cross section of y-vorticity at x = 285 (150 m upwind of the front of the fire). The y component of vorticity for the 10ShapeA simulation is shaded such that positive values of y-vorticity indicate cyclonic rotation about the y-axis, and negative values of y-vorticity indicate anticyclonic rotation about the y-axis.

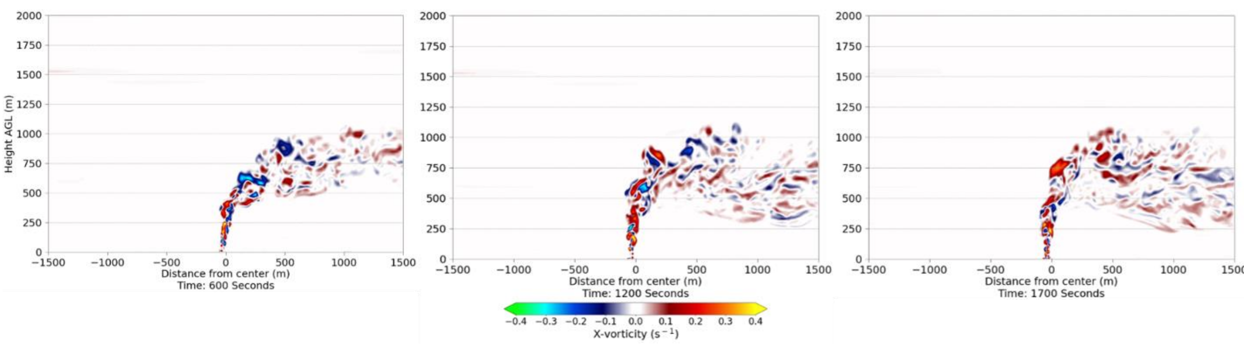

Figure A14. Vertical cross section of x-vorticity through the center of the domain. The x component of vorticity for the 10ShapeA simulation is shaded such that positive values of x-vorticity indicate cyclonic rotation about the x-axis, and negative values of x-vorticity indicate anticyclonic rotation about the x-axis.

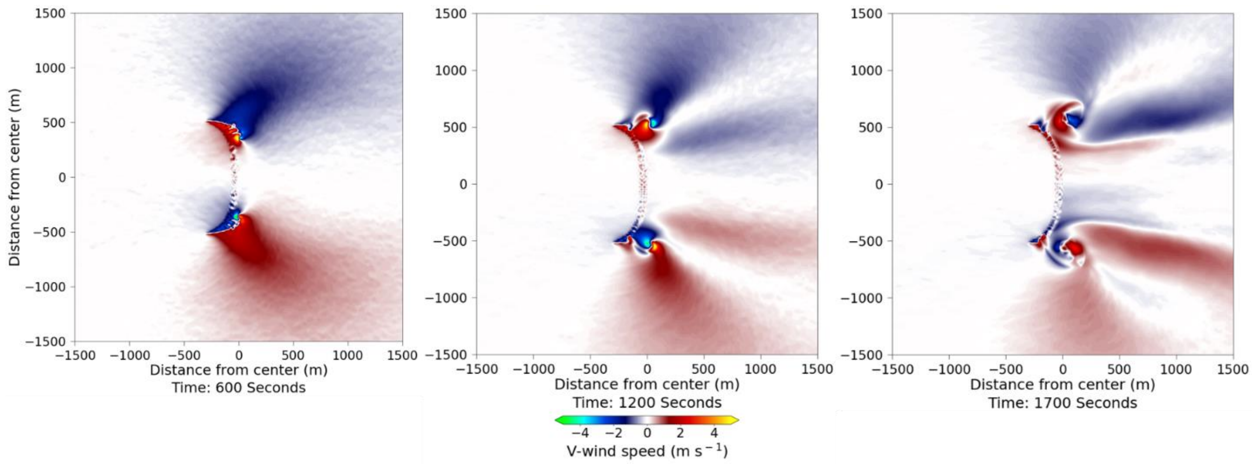

Figure A15. Horizontal cross section of the v-winds at the surface 600, 1200, 1700 s respectively into the 10ShapA simulation. The v-winds at the surface are shaded. Positive values indicate a wind direction from the bottom to the top of the image, negative values indicate a wind direction from the top to the bottom of the image. Convergence of the winds outside the fire arc is associated with the same location of the vertical vorticity minimum/maximum features.

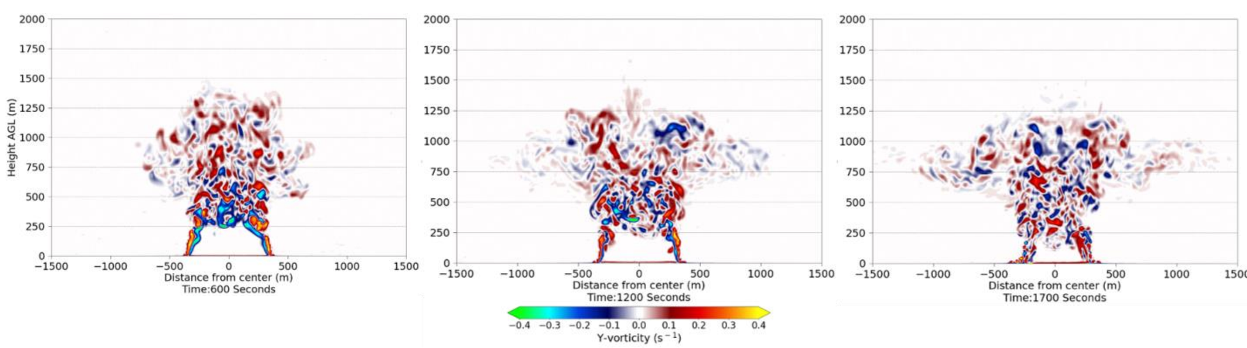

Figure A16. Vertical cross section of y-vorticity at x = 285 (150 m upwind of the front of the fire). The y component of vorticity for the 0ShapeB simulation is shaded such that positive values of y-vorticity indicate cyclonic rotation about the y-axis, and negative values of y-vorticity indicate anticyclonic rotation about the y-axis.

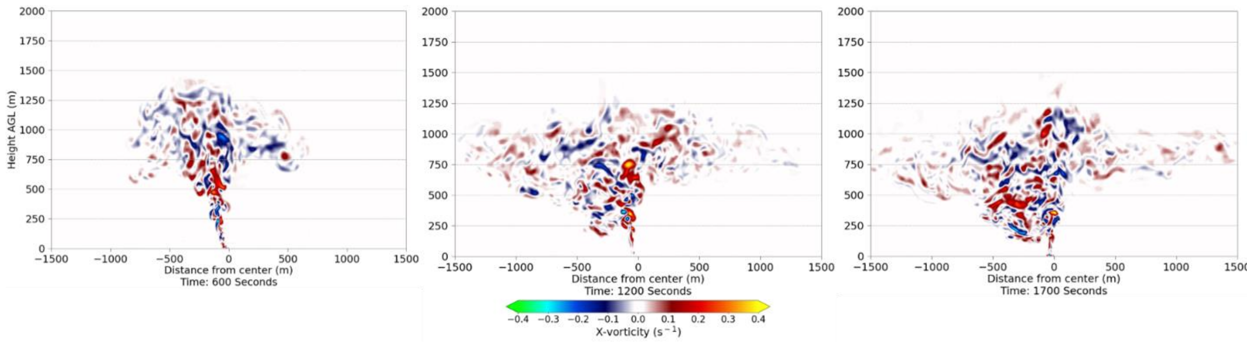

Figure A17. Vertical cross section of x-vorticity through the center of the domain. The x component of vorticity for the 0ShapeB simulation is shaded such that positive values of x-vorticity indicate cyclonic rotation about the x-axis, and negative values of x-vorticity indicate anticyclonic rotation about the x-axis.

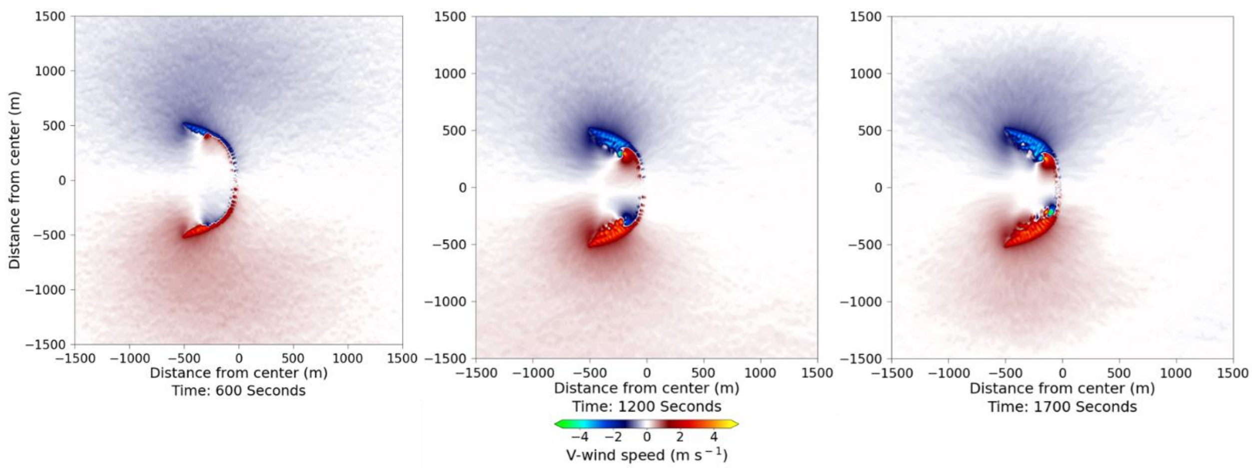

Figure A18. Horizontal cross section of the v-winds at the surface 600, 1200, 1700 s respectively into the 0ShapeB simulation. The v-winds at the surface are shaded. Positive values indicate a wind direction from the bottom to the top of the image, negative values indicate a wind direction from the top to the bottom of the image. Convergence of the winds inside the fire arc is associated with the same location of the vertical vorticity minimum/maximum features.

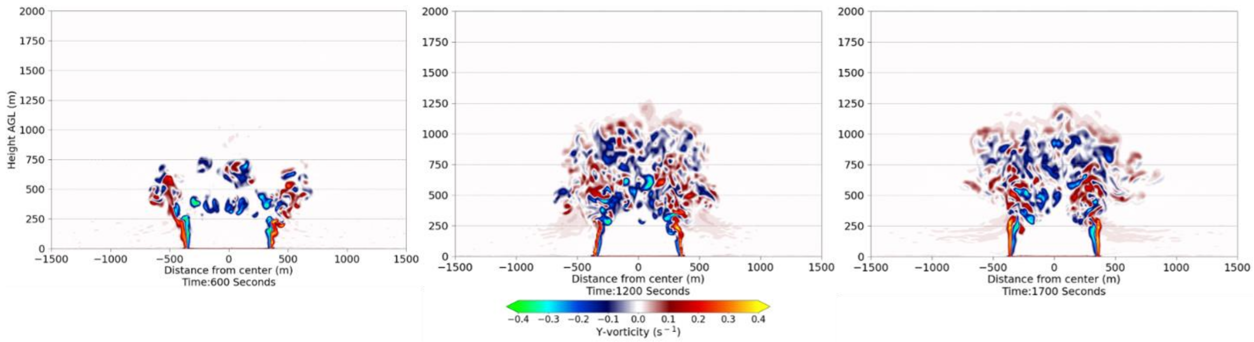

Figure A19. Vertical cross section of y-vorticity at x = 285 (150 m upwind of the front of the fire). The y component of vorticity for the %ShapeB simulation is shaded such that positive values of y-vorticity indicate cyclonic rotation about the y-axis, and negative values of y-vorticity indicate anticyclonic rotation about the y-axis.

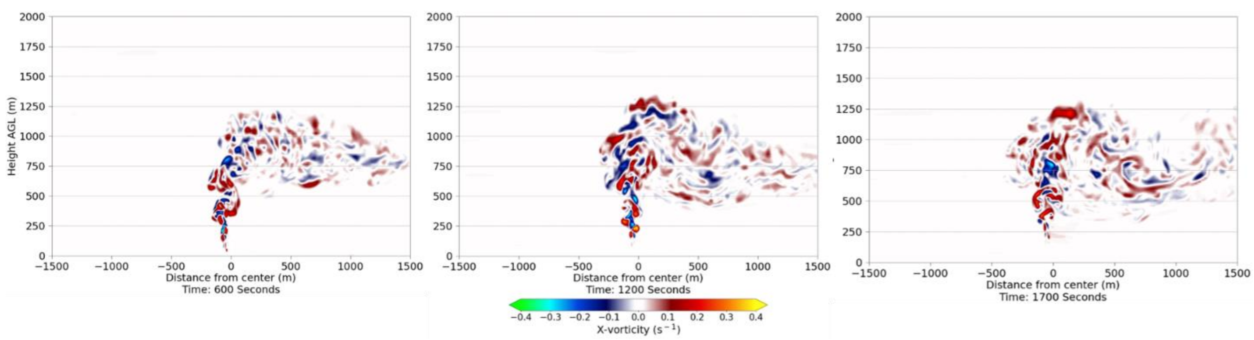

Figure A20. Vertical cross section of x-vorticity through the center of the domain. The x component of vorticity for the 5ShapeB simulation is shaded such that positive values of x-vorticity indicate cyclonic rotation about the x-axis, and negative values of x-vorticity indicate anticyclonic rotation about the x-axis.

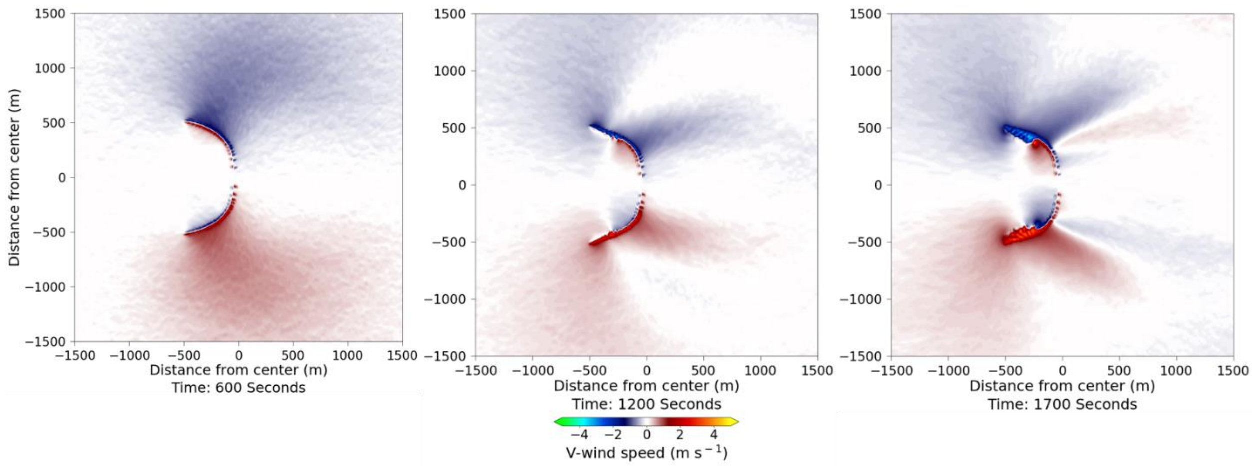

Figure A21. Horizontal cross section of the v-winds at the surface 600, 1200, 1700 s respectively into the 5ShapeB simulation. The v-winds at the surface are shaded. Positive values indicate a wind direction from the bottom to the top of the image, negative values indicate a wind direction from the top to the bottom of the image. Convergence of the winds inside the fire arc is associated with the same location of the vertical vorticity minimum/maximum features.

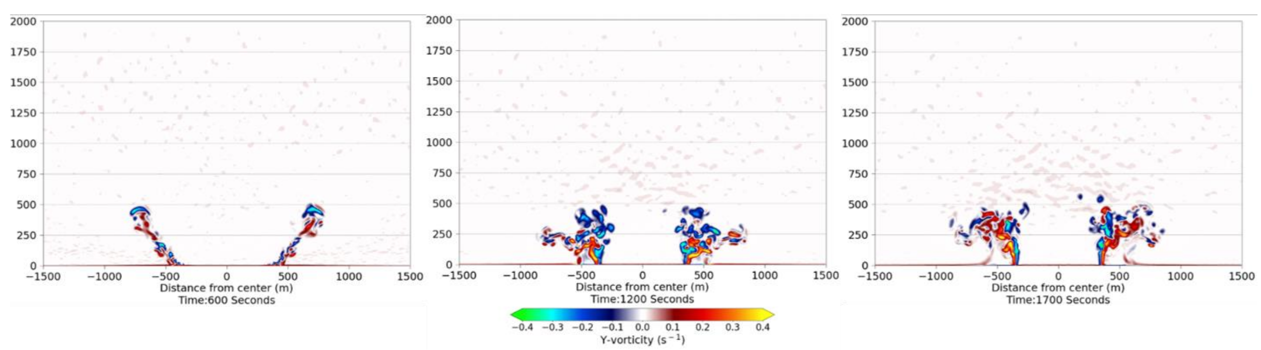

Figure A22. Vertical cross section of y-vorticity at x = 285 (150 m upwind of the front of the fire). The y component of vorticity for the 10ShapeB simulation is shaded such that positive values of y-vorticity indicate cyclonic rotation about the y-axis, and negative values of y-vorticity indicate anticyclonic rotation about the y-axis.

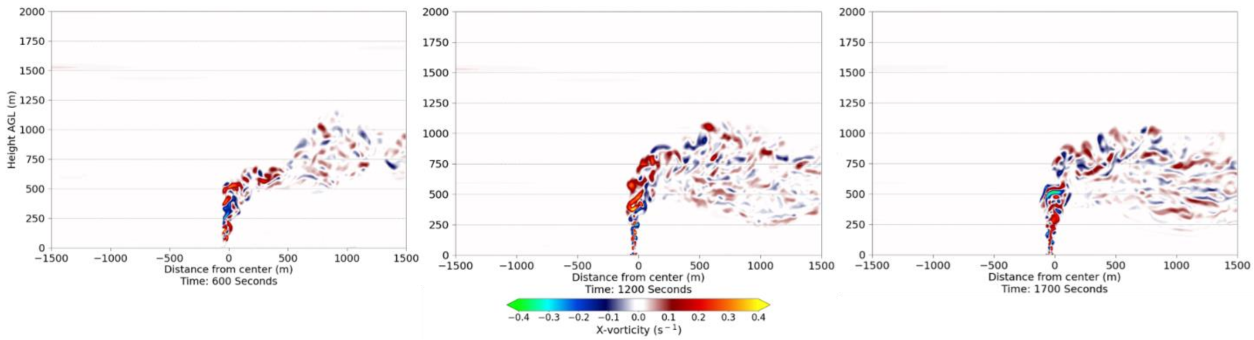

Figure A23. Vertical cross section of x-vorticity through the center of the domain. The x component of vorticity for the 10ShapeB simulation is shaded such that positive values of x-vorticity indicate cyclonic rotation about the x-axis, and negative values of x-vorticity indicate anticyclonic rotation about the x-axis.

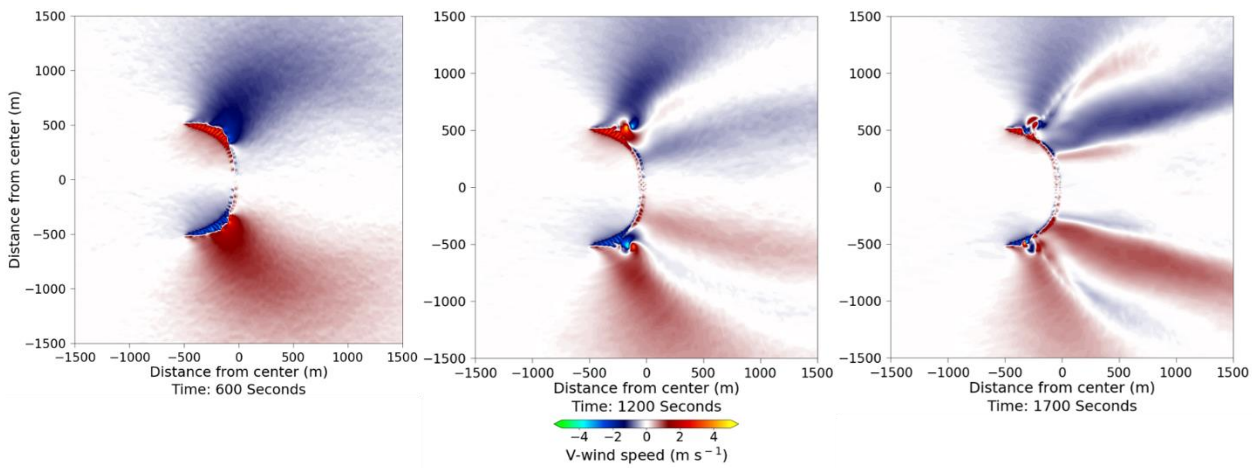

Figure A24. Horizontal cross section of the v-winds at the surface 600, 1200, 1700 s respectively into the 10ShapeB simulation. The v-winds at the surface are shaded. Positive values indicate a wind direction from the bottom to the top of the image, negative values indicate a wind direction from the top to the bottom of the image. Convergence of the winds outside the fire arc is associated with the same location of the vertical vorticity minimum/maximum features.

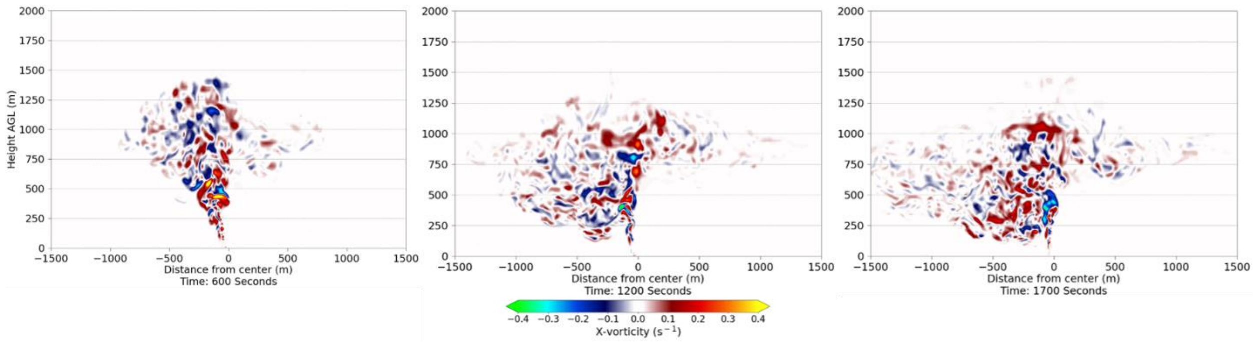

Figure A25. Vertical cross section of x-vorticity through the center of the domain. The x component of vorticity for the 0ShapeC simulation is shaded such that positive values of x-vorticity indicate cyclonic rotation about the x-axis, and negative values of x-vorticity indicate anticyclonic rotation about the x-axis.

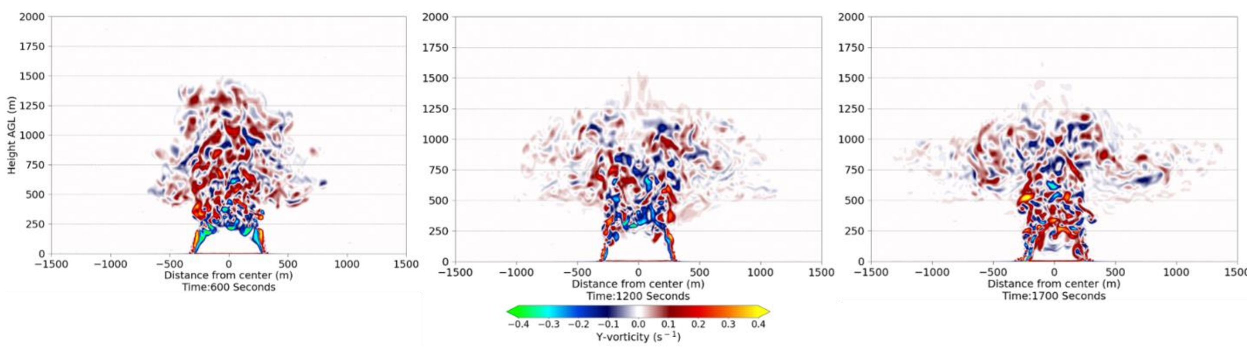

Figure A26. Vertical cross section of y-vorticity at x = 285 (150 m upwind of the front of the fire). The y component of vorticity for the 0ShapeC simulation is shaded such that positive values of y-vorticity indicate cyclonic rotation about the y-axis, and negative values of y-vorticity indicate anticyclonic rotation about the y-axis.

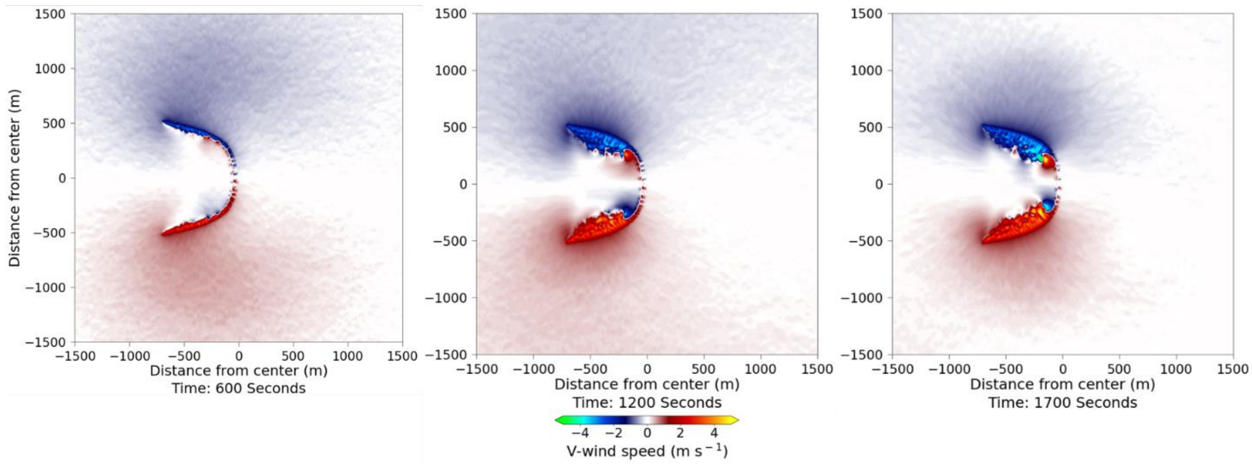

Figure A27. Horizontal cross section of the v-winds at the surface 600, 1200, 1700 s respectively into the 0ShapeC simulation. The v-winds at the surface are shaded. Positive values indicate a wind direction from the bottom to the top of the image, negative values indicate a wind direction from the top to the bottom of the image. Convergence of the winds inside the fire arc is associated with the same location of the vertical vorticity minimum/maximum features.

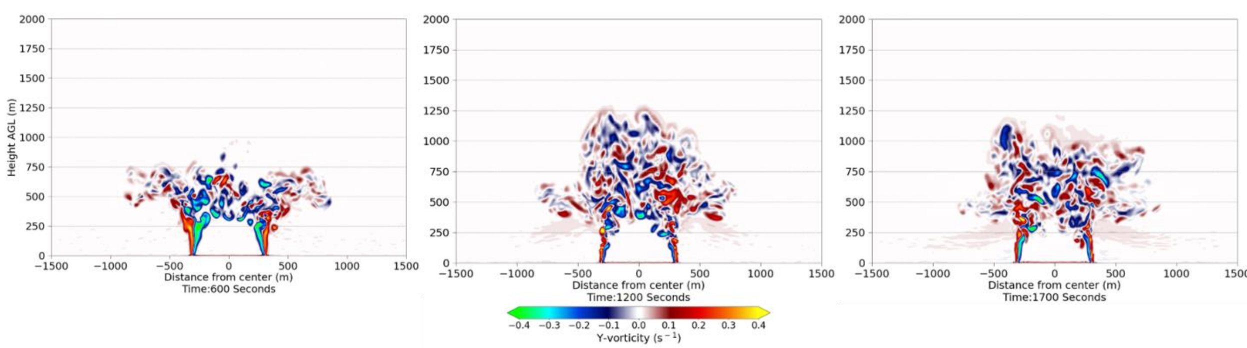

Figure A28. Vertical cross section of y-vorticity at x = 285 (150 m upwind of the front of the fire). The y component of vorticity for the 5ShapeC simulation is shaded such that positive values of y-vorticity indicate cyclonic rotation about the y-axis, and negative values of y-vorticity indicate anticyclonic rotation about the y-axis.

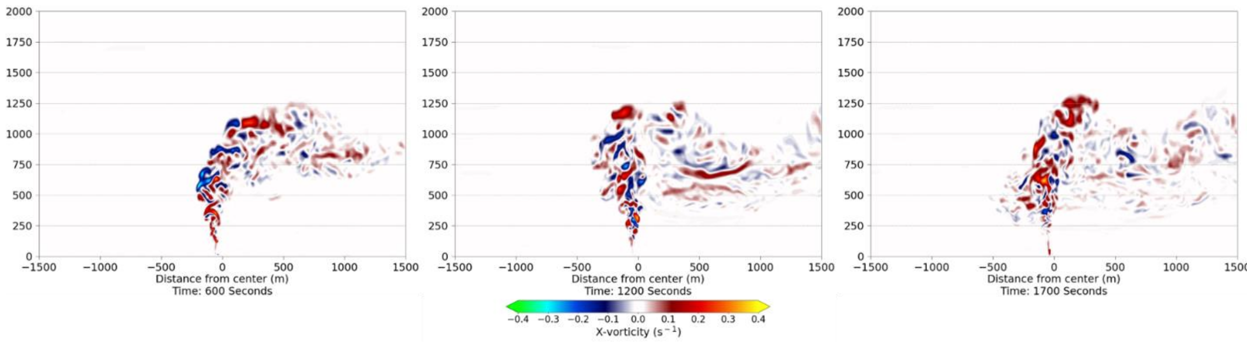

Figure A29. Vertical cross section of x-vorticity through the center of the domain. The x component of vorticity for the 5ShapeC simulation is shaded such that positive values of x-vorticity indicate cyclonic rotation about the x-axis, and negative values of x-vorticity indicate anticyclonic rotation about the x-axis.

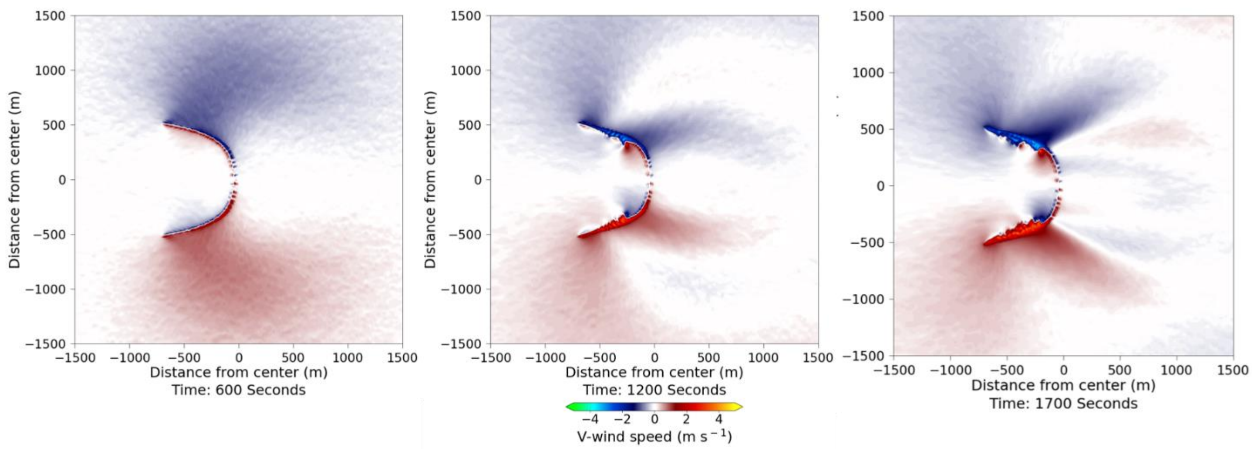

Figure A30. Horizontal cross section of the v-winds at the surface 600, 1200, 1700 s respectively into the 5ShapeC simulation. The v-winds at the surface are shaded. Positive values indicate a wind direction from the bottom to the top of the image, negative values indicate a wind direction from the top to the bottom of the image. Convergence of the winds inside the fire arc is associated with the same location of the vertical vorticity minimum/maximum features.

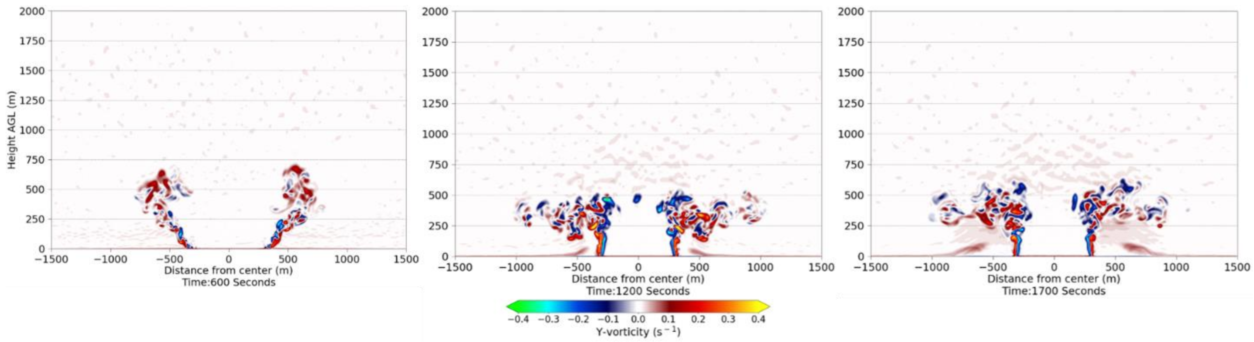

Figure A31. Vertical cross section of y-vorticity at x = 285 (150 m upwind of the front of the fire). The y component of vorticity for the 10ShapeC simulation is shaded such that positive values of y-vorticity indicate cyclonic rotation about the y-axis, and negative values of y-vorticity indicate anticyclonic rotation about the y-axis.

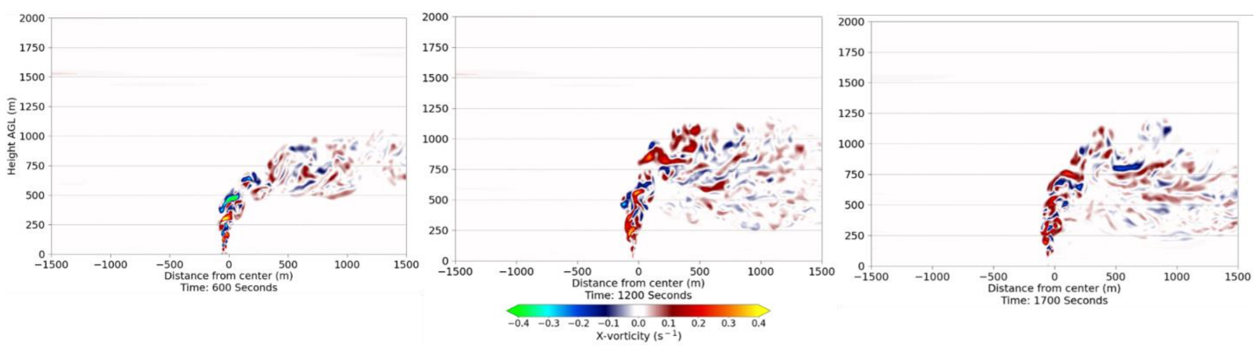

Figure A32. Vertical cross section of x-vorticity through the center of the domain. The x component of vorticity for the 10ShapeC simulation is shaded such that positive values of x-vorticity indicate cyclonic rotation about the x-axis, and negative values of x-vorticity indicate anticyclonic rotation about the x-axis.

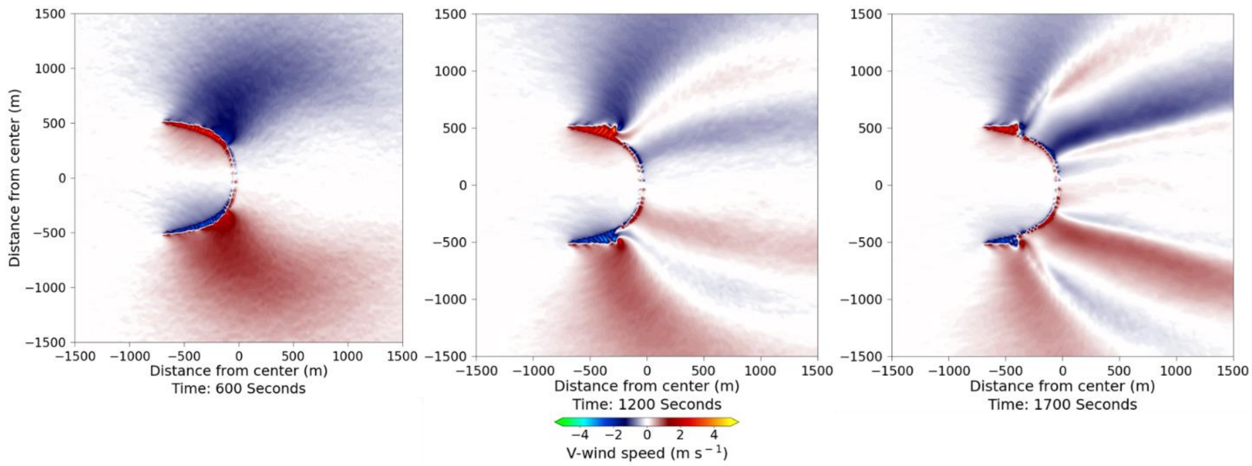

Figure A33. Horizontal cross section of the v-winds at the surface 600, 1200, 1700 s respectively into the 10ShapeC simulation. The v-winds at the surface are shaded. Positive values indicate a wind direction from the bottom to the top of the image, negative values indicate a wind direction from the top to the bottom of the image. Convergence of the winds outside the fire arc is associated with the same location of the vertical vorticity minimum/maximum features. Linear bands of convergence form throughout the simulation that are associated with the linear bands of convergence seen in the u-wind.

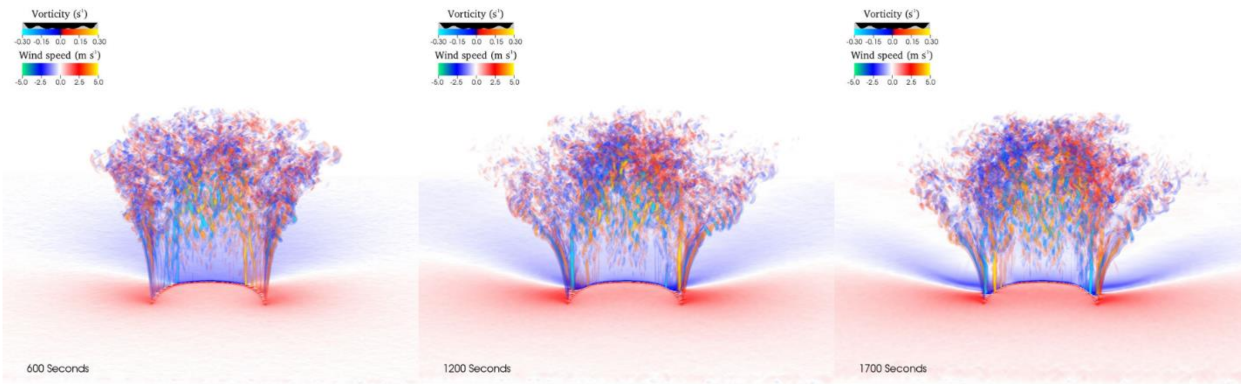

Figure A34. Upwind view of a three-dimensional volume render of vertical vorticity at 600, 1200, 1700 s into the 10ShapeC simulations. The surface is shaded by the perturbations from background u-wind and the volume is shaded by values of vertical vorticity. Positive values of vertical vorticity indicate cyclonic rotation, and negative values of vertical vorticity indicate anticyclonic rotation.

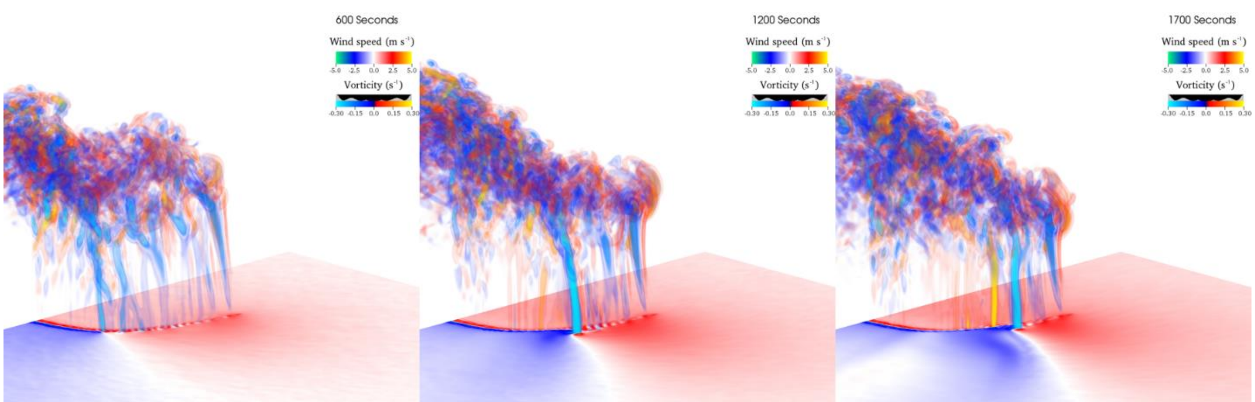

Figure A35. Oblique view of a three-dimensional volume render of vertical vorticity at 600, 1200, 1700 s into the 10ShapeC simulations. The surface is shaded by the perturbations from background u-wind and the volume is shaded by values of vertical vorticity. Positive values of vertical vorticity indicate cyclonic rotation, and negative values of vertical vorticity indicate anticyclonic rotation.

BIBLIOGRAPHY

BIBLIOGRAPHY

Albini, F. A., 1976: Estimating wildfire behaviour and effects. USDA For. Serv. Gen. Tech. Rep. INT-30, Washington, DC.

Albini, F. A., 1982: Response of free-burning fires to non-steady wind. *Combustion Science and Technology*, **29**(3–6), 225–241. doi:10.1080/ 00102208208923599.

Alexander, M. E., 1985: Estimating the length-to-breadth ratio of elliptical forest fire patterns. pp. 287-304 *Proc. 8th Conf. Fire and Forest Meteor*.

Anderson, D. H., E. A. Catchpole, N. J. de Mestre, and T. Parkes, 1982: Modelling the spread of grass fires. *Aust. Math. J.*, Ser. B, 23: 451-466. https://doi.org/10.1017/S0334270000000394.

Bryan, G. H., and J. M. Fritsch, 2002: A benchmark simulation for moist nonhydrostatic numerical models. *Mon. Wea. Rev.*, **130,** 2917-2928.

Byram, G. M., 1954: Atmospheric conditions related to blowup fires. USDA Forest Service, Southeastern Forest Experiment Station, Paper 35. (Asheville, NC)

Byram, G. M., R. M. Nelson, 1951: The possible relation of air turbulence to erratic fire behavior in the South-east. *Fire Control Notes* **12**(3), 1–8. [Republished in *Fire Management Today* **63**(3), 46–51]

Cheney, N. P., J. S. Gould, 1995: Fire growth in grassland fuels. *Int. J. Wildland Fire*, **5**, 237–247. doi:10.1071/WF9950237

Cheney, N. P., J. S. Gould, W.R. Catchpole, 1993: The influence of fuel, weather and fire shape variables on fire spread in grasslands. *Int. J. Wildland Fire*, **3**, 31–44. doi:10.1071/WF9930031

Clark T. L., M. A. Jenkins, J. Coen, D. Packham, 1996a: A coupled atmosphere–fire model: convective feedback on fire-line dynamics. *J. Appl. Meteor.*, **35**(6), 875–901. doi:10.1175/1520-0450(1996) 035,0875:ACAMCF.2.0.CO;2.

Clements, C. B., S. Zhong, S. Goodrick, J. P. Li, X. Bian, W. E. Heilman, and M. Patel, 2007: Observing the dynamics of wildland grass fires: FireFlux—a field validation experiment. *Bull. Amer. Meteor. Soc.*, **88**, 1369–1382, doi:10.1175/BAMS-88-9-1369.

Coen, J. L., M. Cameron, J. Michalakes, E.G. Patton, P.J.Riggan, and K.M. Yedinak, 2013: WRF-Fire: Coupled weather-wildland fire modeling with the Weather Research and Forecasting model, *J.Appl.Meteorol.Climatol*., **52**, 16–38, doi:10.1175/JAMC-D-12-023.1.

Coffer, B. E., M. D. Parker, J. M. L. Dahl, L. J. Wicker, and A. J. Clark, 2017: Volatility of tornadogenesis: An ensemble of simulated nontornadic and tornadic supercells in VORTEX2 environments. *Mon. Wea. Rev.*, **145,** 4605-4625, doi:10.1175/MWR-D-17-0152.1.

Green, D. G., A. M. Gill, and I. R. Noble, 1983. Fire shapes and the adequacy of fire-spread models. *Ecol. Modelling*, **20**: 33-45. https://doi.org/10.1016/0304-3800(83)90030-3.

Heilman W. E., J. D. Fast, 1992: Simulation of horizontal roll vortex development above lines of extreme surface heating. *Int. J. Wildland Fire*, **2**(2), 55–68. doi:10.1071/WF9920055

Jenkins, M.A., R. Sun, S. K. Krueger, J. J. Charney, and M. A. Zulauf, 2007: Effect of vertical wind shear on grassfire evolution. in Proceedings of the 7th Symposium of Forest and Fire Meteorology, Bar Harbor, Me, USA, October 2007.

Kiefer M. T., Y. L. Lin, J. J. Charney, 2008: A study of two-dimensional dry convective plume modes with variable critical level height. *J. Atmos. Sci.*, **65**, 448–469. doi:10.1175/2007JAS2301.1

Kiefer M. T., M. D. Parker, J. J. Charney, 2009: Regimes of dry convection above wildfires: idealized numerical simulations and dimensional analysis. *J. Atmos. Sci.*, **66**, 806–836. doi:10.1175/ 2008JAS2896.1

Kiefer M. T., M. D. Parker, J. J. Charney, 2010: Regimes of Dry Convection above Wildfires: Sensitivity to Fire Line Details. *J. Atmos. Sci.*, **67**, 611-632. 10.1175/2009JAS3226.1.

Linn, R. R., F. H. Harlow, 1997: *FIRETEC: A transport description of wildfire behavior*. United States: N. p., 1997. Web. doi:10.2172/505313.

MacIntosh, C. W. and M. D. Parker, 2017: The 6 May 2010 elevated supercell during VORTEX2. *Mon. Wea. Rev.*, **145,** 2635-2657, doi:10.1175/MWR-D-16-0329.1.

McGrattan, K. B., 2002: Fire Dynamics Simulator Technical Reference Guide Volume 1: Mathematical Model. NISTIR, Special Publication 1018. (Gaithersburg, MD)

Mell W., M. A. Jenkins, J. Gould, P. Cheney, 2007: A physics-based approach to modeling grassland fires. *Int. J. Wildland Fire* **16**, 1–22. https://doi.org/10.1071/WF06002.

Miller, M. J., A. A. White, 1984: On the nonhydrostatic equations in pressure and sigma coordinates. *Quart. J. Roy. Meteor. Soc.*, **110**, 505-533.

Orf, L., R. Wilhelmson, B. Lee, C. Finley, and A. Houston, 2016: Evolution of a long-track violent tornado within a simulated supercell. *Bull. Amer. Meteor. Soc.,* in press, doi:10.1175/BAMS-D-15-00073.1.

Peet, G. B., 1967: The shape of mild fires in Jarrah forest. *Aust. For.*, **31**: 121-127. DOI: 10.1080/00049158.1967.10675433.

Potter, B. E., 2012: Atmospheric interactions with wildland fire behaviour – I. Basic surface interactions, vertical profiles and synoptic structures, *Int. J. Wildland Fire*, **21**, 779–801. https://doi.org/10.1071/WF11128.

Rothermel, R. C., 1972: A mathematical model for predicting fire spread in wildland fuels. USDA Forest Service, Intermountain Forest and Range Experiment Station, Research Paper INT-115. (Ogden, UT)

Rothermel, R. C., H. E. Anderson, 1966: Fire spread characteristics determined in the laboratory. USDA Forest Service, Intermountain Forest and Range Experiment Station, Research Paper INT-30. (Ogden, UT)

Simpson, C., M. Katurji, M. T. Kiefer, S. Zhong, J. J. Charney, W. E. Heilman, and X. Bian, 2013: Atmosphere-fire simulation of effects of low-level jets on pyro-convective plume dynamics. In J. Piantadosi, R. Anderssen, and J. Boland (Eds.), 20th International Congress of Modelling and Simulation. AMS, Adeleaide, Australia, 13-18 November 2013

Simpson, C., J. J. Sharpels, J. P. Evans, 2014: Resolving vorticity-driven lateral fire spread using the WRF-Fire coupled atmosphere-fire numerical model. *Nat. Hazards Earth Syst. Sci.*, **14**, 2359-2371, doi:10.5194/nhess-14-2359-2014.

Steiner, J. T., 1976: Blowup fires – the Byram wind profile. *Aust. Meteor. Mag.* **24**(3), 139–142.

Stevens, B., C. -H. Moeng, and P. P. Sullivan, 1999: Large-eddy simulations of radiatively driven convection: sensi-tivities to the representation of small scales. *J. Atmos. Sci.*, 56, 3963–3984, doi:10.1175/1520-0469(1999)056,3963:LESORD>2.0.CO;2.

Sun, R., S. K. Krueger, M. A. Jenkins, M. A. Zulauf, and J. J. Charney, 2009: The importance of fire-atmosphere coupling and boundary-layer turbulence to wildfire spread. *Int. J. Wildland Fire*, **18**, 50–60, doi:10.1071/WF07072.

Van Wagner C. E., 1969: A simple fire-growth model. *For. Chron.*, **45**(2): 103-104. https://doi.org/10.5558/tfc45103-2.

Wicker, L. J., and W. C. Skamarock, 1998: A time-splitting scheme for the elastic equations incorporating secondorder Runge–Kutta time differencing. *Mon. Wea. Rev.*, **126**, 1992–1999, doi:10.1175/1520-0493(1998)126 2.0.CO;2.

Xue, M., A. J. Thorpe, 1991: A mesoscale numerical model using the nonhydrostatic sigma-coordinate equations: Model experiments with dry mountain flows, *Mon. Wea Rev.*, **119**, 1168-1185.